Running Title: Dissociation of lipid transfer activities of MTTP

A missense mutation dissociates triglyceride and phospholipid transfer activities in zebrafish and human microsomal triglyceride transfer protein

Meredith H. Wilson[1], Sujith Rajan[2], Aidan Danoff[1,3], Richard J. White[4,5], Monica R. Hensley[1], Vanessa H. Quinlivan[1], James H. Thierer[1,3], Elisabeth M. Busch-Nentwich[4,5], M. Mahmood Hussain[2,*], Steven A. Farber[1,3,*]

1 Carnegie Institution for Science Department of Embryology, Baltimore, MD 21218
2 New York University Winthrop Hospital, Mineola, NY11501
3 Johns Hopkins University Department of Biology, Baltimore, MD 21218
4 Wellcome Sanger Institute, Wellcome Genome Campus, Hinxton, Cambridge, CB101SA, UK
5 Department of Medicine, University of Cambridge, Cambridge, CB2 0QQ, UK

Footnote:
*Corresponding Author: Steven A. Farber farber@carnegiescience.edu
M. Mahmood Hussain Mahmood.Hussain@nyulangone.org

SUMMARY

Microsomal triglyceride transfer protein (MTP) transfers triglycerides and phospholipids and is essential for the assembly of Apolipoprotein B (ApoB)-containing lipoproteins in the endoplasmic reticulum. We have discovered a zebrafish mutant (*mttp*^{c655}) expressing a C-terminal missense mutation (G863V) in Mttp, one of the two subunits of MTP, that is defective at transferring triglycerides, but retains phospholipid transfer activity. Mutagenesis of the conserved glycine in the human MTTP protein (G865V) also eliminates triglyceride but not phospholipid transfer activity. The G863V mutation reduces the production and size of ApoB-containing lipoproteins in zebrafish embryos and results in the accumulation of cytoplasmic lipid droplets in the yolk syncytial layer. However, *mttp*^{c655} mutants exhibit only mild intestinal lipid malabsorption and normal growth as adults. In contrast, zebrafish mutants bearing the previously identified *mttp*^{stl} mutation (L475P) are deficient in transferring both triglycerides and phospholipids and exhibit gross intestinal lipid accumulation and defective growth. Thus, the G863V point mutation provides the first evidence that the triglyceride and phospholipid transfer functions of a vertebrate MTP protein can be separated, arguing that selective inhibition of the triglyceride transfer activity of MTP may be a feasible therapeutic approach for dyslipidemia.

Keywords: MTP, MTTP, ApoB, lipid transfer, zebrafish, yolk

INTRODUCTION

In vertebrates, Apolipoprotein B-containing lipoproteins (B-lps) are produced by the intestine and liver and transport lipid and fat-soluble vitamins to the peripheral tissues through the circulation. Lipoproteins are composed of a neutral core of triglyceride (TG) and cholesteryl esters surrounded by a monolayer of phospholipid, free cholesterol and sphingomyelin. B-lps contain one apolipoprotein B (ApoB) scaffold protein embedded in the phospholipid monolayer as well as other exchangeable lipoproteins (Hussain et al., 1996; Schumaker et al., 1994). B-lp assembly occurs in the endoplasmic reticulum (ER) and requires the activity of microsomal triglyceride transfer protein (MTP) (Hussain et al., 2003b; Patel and Grundy, 1996; Wetterau and Zilversmit, 1986). As ApoB is translated and translocated into the lumen of the ER, MTP physically interacts with and transfers lipids to ApoB to form primordial lipoproteins (Bradbury et al., 1999; Hussain et al., 2003b; Patel and Grundy, 1996; Wu et al., 1996). MTP may also aid in the formation of TG-rich lumenal lipid droplets that are believed to fuse to the primordial lipoproteins, thus increasing the size of nascent lipoproteins (Alexander et al., 1976; Boren et al., 1994; Hamilton et al., 1998; Kulinski et al., 2002; Raabe et al., 1999; Wang et al., 1997).

MTP is a heterodimer of the large 97-kDa M subunit (microsomal triglyceride transfer protein, MTTP) and the small 58-kDa P subunit protein disulfide isomerase (PDI)(Wetterau et al., 1990). Mutations in the *MTTP* gene that prevent lipid transfer and ApoB secretion cause the disease Abetalipoproteinemia (OMIM 200100), characterized by a virtual absence of plasma B-lps (Kane, 1995; Sharp et al., 1993; Shoulders et al., 1993; Wetterau et al., 1992). Patients exhibit fat malabsorption, low plasma triglyceride, and cholesterol levels as well as fat-soluble vitamin deficiencies (Kane, 1995; Lee and Hegele, 2014; Walsh and Hussain, 2016). Without adequate supplementation of essential fatty acids and fat-soluble vitamins, these patients can develop a variety of complications including neurological, opthalmological, and hematological disorders (Kane, 1995; Lee and Hegele, 2014).

Vertebrate MTP can transfer triacylglycerol, diacylglycerol, phospholipid, cholesteryl ester, ceramide, and sphingomyelin between vesicles *in vitro* (Athar et al., 2004; Iqbal et al., 2015; Jamil et al., 1995; Rava et al., 2005; Wetterau and Zilversmit, 1984, 1985). Kinetic studies suggest that MTP transiently interacts with membranes, acquires lipids, and then delivers these

lipids to an acceptor membrane. The transfer of lipids occurs down a concentration gradient and does not require energy (Atzel and Wetterau, 1993, 1994). While vertebrate MTP predominantly transfers TG (Rava et al., 2005; Wetterau and Zilversmit, 1985), the Drosophila orthologue of MTP lacks TG transfer activity (Rava et al., 2006), has phospholipid transfer activity and supports secretion of vertebrate ApoB (Khatun et al., 2012; Rava and Hussain, 2007; Rava et al., 2006; Sellers et al., 2003). A further analysis of MTTP orthologues in divergent species, including nematodes, insects, fish, and mammals, indicates that all orthologues bind PDI, localize to the ER, and support human ApoB secretion (Rava and Hussain, 2007). However, only vertebrate MTP orthologues exhibit TG transfer activity, suggesting that phospholipid transfer activity was the original function of MTP orthologues and that neutral lipid transfer first evolved in fish (Rava and Hussain, 2007).

Here we describe a hypomorphic missense mutation in the C-terminal domain of zebrafish *mttp* (G863V) that decreases the production and size of B-lps *in vivo*, but has minimal effects on lipid malabsorption in the intestine and no effect on growth. Biochemical characterization of the G863V allele indicates that it is defective in triglyceride transfer activity, but retains phospholipid transfer activity. Further, we show that mutation of the conserved glycine at position 865 in human *MTTP* also selectively abolishes triglyceride transfer activity. Taken together, these data provide the first evidence that the lipid transfer functions of a vertebrate MTP can be biochemically dissociated and argues that phospholipid transfer activity is sufficient for absorption of dietary lipid.

RESULTS

The c655 allele is a missense mutation in mttp. During routine screening, we identified zebrafish embryos with opaque yolks (Figure 1A). In contrast to the translucent yolks of wild-type fish, when illuminated by transmitted light, the mutant yolks appear dark (Figure 1A) and, with incident light, appear off-white (Figure 1— figure supplement 1A). The phenotype was found to be present in Mendelian ratios (Figure 1A), suggesting the presence of a homozygous recessive mutation. This new allele is identified as Carnegie allele *c655*. To map the location of the causative mutation, we did RNA sequencing of 23 opaque-yolk *c655* mutants and 23 translucent-yolk siblings and performed a Euclidean distance mapping analysis using the Mutation Mapping Analysis Pipeline for Pooled RNA-seq (MMAPPR)(Hill et al., 2013). The

110 Loess fit to the mapping scores (Euclidean Distance[4]) (Figure 1B, top) indicated the c655
111 mutation was located on Chromosome 1 and lay in the region between 9-20 MB (Figure 1B,
112 bottom). Single nucleotide variants (SNVs) present in this 11MB region in *c655* mutant embryos
113 were assessed for their effect on annotated genes using the Ensembl Variant Effect Predictor
114 (McLaren et al., 2016), including using the Sorting Intolerant from Tolerant algorithm (SIFT)
115 (Sim et al., 2012), to predict the impact of changes on protein-coding sequence (tolerated or
116 deleterious). We extracted variants that alter the protein-coding sequence as candidates for the
117 causal mutation (223 variants in 64 genes, of which 42 are missense variants predicted to be
118 deleterious; Supplementary File 1).
119

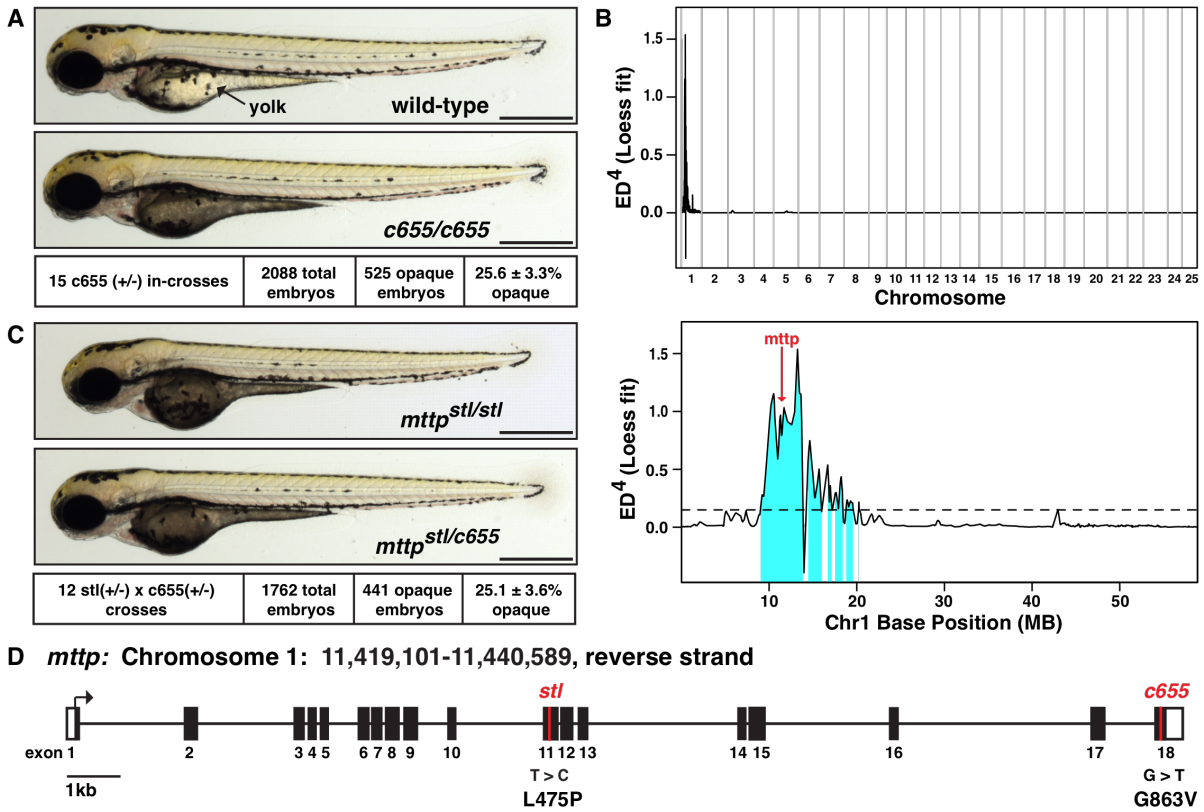

120
121
122
123 **Figure 1: The *c655* allele is a missense mutation in the M-subunit of microsomal**
124 **triglyceride transfer protein.** (A) Representative images of wild-type (top) and homozygous
125 mutant (middle) c655 zebrafish embryos at 3 days post fertilization (dpf); Scale = 500 μm. The
126 dark/opaque yolk phenotype segregated with a Mendelian ratio consistent with a homozygous
127 recessive mutation (bottom), mean +/- SD. (B) Euclidean distance mapping analysis plots

128 produced by MMAPPR (Hill et al., 2013), showing the likely genomic region of the *c655*
129 mutation: plot of the LOESS fit to the mapping scores (Euclidean Distance[4]) across all 25
130 chromosomes (top) and expanded view of chromosome 1(GRCz10: CM002885.1)(bottom).
131 Red arrow shows the position of the G>T missense mutation in *mttp* (ENSDARG00000008637,
132 position 11,421,261(GRCz10). (C) Representative images of a homozygous mutant zebrafish
133 embryo carrying the previously described *stalactite* (*stl*) missense mutation in *mttp* (Avraham-
134 Davidi et al., 2012)(top) and a trans-heterozygous $mttp^{stl/c655}$ embryo (middle); 3 dpf, scale = 500
135 μm. The dark/opaque yolk phenotype is present at expected ratios (bottom) and genotyping
136 confirms only embryos with opaque yolks are trans-heterozygous for the *mttp* alleles. (D)
137 Depiction of the *mttp* gene structure highlighting the locations of the *stl* (L475P) (position
138 11,431,645, GRCz10, transcript mtp-204 (ENSDART00000165753.2) nucleotide 2588) and
139 *c655* (G863V) (nucleotide 1424) missense alleles in exon 11 and 18, respectively.
140
141

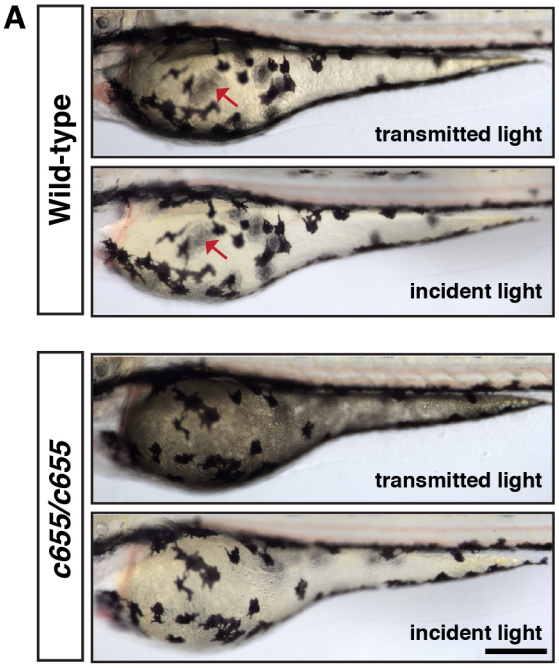

142
143
144 **Figure 1 – figure supplement 1: Lipid droplets block light transmission through the yolk**
145 **of the embryo.** (A) Wild-type and *c655* mutant embryos were imaged at 3 dpf using either
146 transmitted light (illumination below the fish) or incident light (illumination from above the fish).
147 The wild-type embryos are translucent; the pigment cells on the opposite side of the embryo
148 (red arrow) are visible through the yolk with both light sources. The yolk is opaque in the

149 mutants; it appears dark with transmitted light and white with incident light. Pigment cells on the
150 opposite side of the embryo are barely visible in mutant embryos, regardless of light source.
151 Scale = 200 μM.
152
153
154 One of the SNVs linked to the *c655* phenotype was a missense mutation predicted to be
155 deleterious in exon 18 of the microsomal triglyceride transfer protein gene
156 (ENSDARG00000008637, Chr1:11,421,261 GRCz10). A previously identified missense
157 mutation in exon 11 of zebrafish *mttp*, stalactite (*stl*), also presents with an opaque yolk
158 phenotype (Figure 1C, top) (Avraham-Davidi et al., 2012), suggesting that the *c655* opaque yolk
159 phenotype might result from this newly identified missense mutation in *mttp*. To test this
160 hypothesis, we performed complementation crosses between $mttp^{c655/+}$ heterozygous fish and
161 $mttp^{stl/+}$ heterozygous fish. The *c655* mutation failed to complement the $mttp^{stl}$ mutation, as one-
162 quarter of the embryos in these crosses displayed the opaque yolk phenotype (Figure 1C,
163 bottom). All of the embryos exhibiting opaque yolks were heterozygous for both the $mttp^{stl}$ and
164 the *c655* mutation in *mttp*. This strongly argues that the G/T SNV in exon 18 of *mttp* is the
165 causative allele for the *c655* opaque yolk phenotype. This was further confirmed by rescuing
166 the *c655* opaque yolk phenotype with injections of a wild-type mttp-FLAG plasmid at the 1-cell
167 stage (Figure 1— figure supplement 2).
168

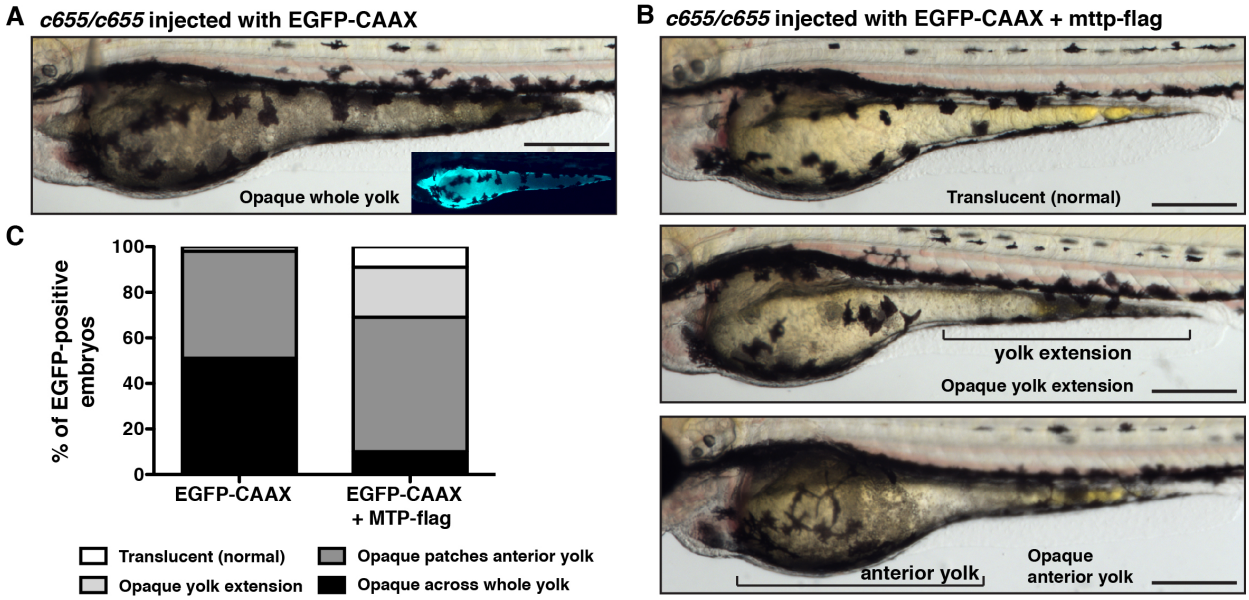

169
170
171

172 **Figure 1 – figure supplement 2: Expression of wild-type zebrafish *mttp*-FLAG rescues**
173 **the opaque yolk phenotype in *mttp*$^{c655/c655}$ embryos.** One-cell stage *mttp*$^{c655/c655}$ embryos
174 were co-injected with CMV: *mttp*-FLAG and the CMV: *eGFP-CAAX* plasmid, or CMV: *eGFP-*
175 *CAAX* alone as a control. Embryos expressing eGFP in the YSL were imaged at 3 dpf, and
176 images were blinded and scored for the degree of yolk opacity. (A) Representative image of an
177 *mttp*$^{c655/c655}$ mutant embryo expressing eGFP-CAAX in the YSL and a fully opaque yolk. (B)
178 Examples of injected embryos with varying degrees of yolk opacity (normal translucent yolk,
179 opaque region in the yolk extension, opaque patches in the anterior yolk with or without opaque
180 yolk extension). (C) Images were binned into the four noted categories of yolk opacity. Results
181 represent pooled data from 3 independent experiments, n = 91 control and 102 Mttp-FLAG
182 eGFP-positive embryos total. Chi-square test, $p<0.001$. Scale = 500 μM.
183
184
185 Both the *mttp*^{stl} allele and *mttp*^{c655} allele are missense mutations. The *stl* allele results in the
186 conversion of a leucine to a proline at residue 475 and the *c655* mutation is a glycine to valine
187 mutation in the C-terminus of the protein at residue 863 (total length = 884 residues) (Figure
188 1D). An additional SNV in *mttp* at position Chr1:11,421,300 GRCz10 (T/C) causing a missense
189 mutation (M850T) was identified in *c655* mutants; however, this SNP was not predicted to be
190 deleterious and has been previously noted in the Ensembl zebrafish genome database.
191 Furthermore, no change in mRNA expression was noted for *mttp* in the *mttp*^{c655} mutants in our
192 RNAseq data-set (log2[fold change] = 0.18, adj. p-value = 0.19).
193
194 Although the *mttp*$^{stl/stl}$, *mttp*$^{c655/c655}$, and trans-heterozygous *mttp*$^{stl/c655}$ fish all exhibit opaque
195 yolks, the *mttp*$^{stl/stl}$ mutants have a more severe phenotype, in that their yolks are darker and
196 they retain the opaque phenotype longer during development. The *mttp*$^{c655/c655}$ mutant
197 phenotype is the least severe and the trans-heterozygotes exhibit an intermediate phenotype
198 (Figure 1— figure supplement 3). Encouraged by the differences in embryonic phenotype, we
199 hypothesized that these mutations would provide an opportunity to further dissect the molecular
200 details of MTP function *in vivo*.
201
202

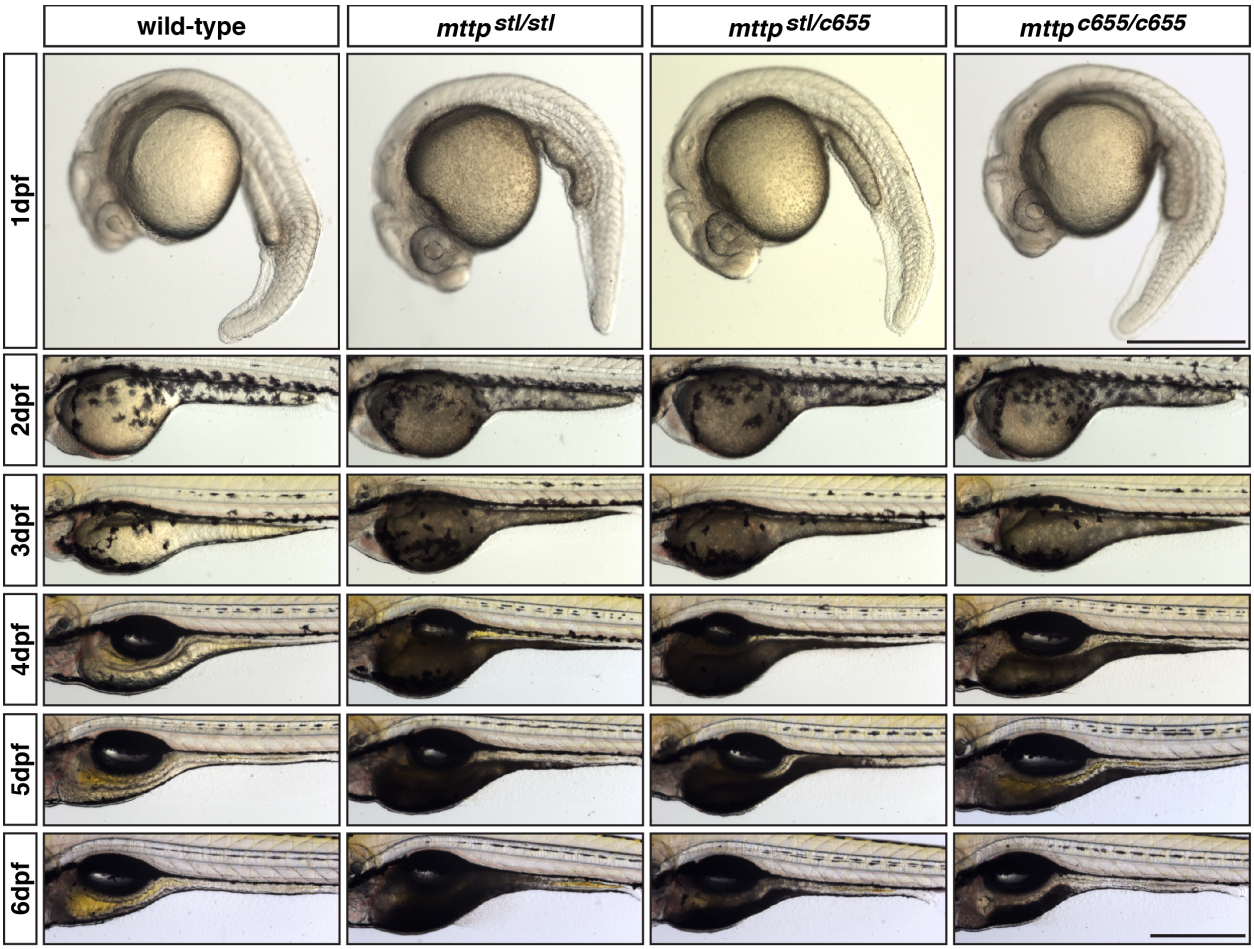

Figure 1 — figure supplement 3: The *stl* and *c655* mttp mutations have differential effects on the degree of yolk opacity during embryonic development. Representative images of wild-type, *mttp*$^{stl/stl}$, *mttp*$^{c655/c655}$ and trans-heterozygous *mttp* $^{stl/c655}$ mutants from 1 dpf to 6 dpf. The *mttp*$^{stl/stl}$ mutants are visibly opaque at 1 dpf and the area of opacity is retained for longer than in *mttp*$^{stl/c655}$ or *mttp*$^{c655/c655}$ mutants. 3 dpf images are the same fish shown in Figure 1. Scale = 500 μM.

Mttp mutants accumulate cytoplasmic lipid droplets in the yolk syncytial layer. As a lecithotrophic organism, zebrafish rely on their maternally-derived yolk as the source of nutrients and building blocks for embryogenesis (Hiramatsu et al., 2015; Mani-Ponset et al., 1996; Vernier and Sire, 1977). The yolk is rich in lipids (Fraher et al., 2016; Miyares et al., 2014; Wiegand, 1996) and following lipolysis and re-esterification, the lipids are packaged into lipoproteins in the ER of the yolk syncytial layer (YSL), a multi-nucleated cytoplasm that

219 surrounds the yolk mass (Figure 2A)(Carvalho and Heisenberg, 2010; Kimmel and Law, 1985;
220 Walzer and Schonenberger, 1979a, b). The zebrafish YSL expresses apolipoprotein B (Otis et
221 al., 2015) and microsomal triglyceride transfer protein (Marza et al., 2005; Schlegel and Stainier,
222 2006). The YSL produces B-lps (Thierer et al., In Press; Vernier and Sire, 1977; Walzer and
223 Schonenberger, 1979a), similar to the intestine (Glickman et al., 1976; Kessler et al., 1970),
224 liver (Mahley et al., 1970), placenta (Madsen et al., 2004), and embryonic yolk sac in mammals
225 (Farese et al., 1996; Plonne et al., 1992). In the mammalian intestine, ApoB mRNA is edited,
226 resulting in a truncated ApoB molecule (ApoB48)(Davidson and Shelness, 2000; Kane et al.,
227 1980); however, there is no evidence for editing in zebrafish, so all B-lp-producing tissues,
228 including the YSL, secrete lipoproteins containing ApoB100 (Thierer et al., In Press).
229
230 When MTP is mutated or absent, B-lp production is reduced or absent and TG accumulates in
231 cytoplasmic lipid droplets (LDs) instead (Khatun et al., 2012; Raabe et al., 1999). We have
232 previously shown that accumulation of LDs in intestinal enterocytes of zebrafish larvae fed a
233 high-fat meal causes the gut to be opaque (Otis and Farber, 2016)(Figure 2 – figure supplement
234 1), most likely due to the lipid droplets' ability to scatter light (Hwang et al., 2018; Michels et al.,
235 2008). Therefore, we hypothesized that the yolk opacity in the *mttp* mutant embryos is due to
236 aberrant accumulation of LDs in the cytoplasm of the YSL. Using transmission electron
237 microscopy, we found that the YSL in the wild-type embryos contains very few, if any, canonical
238 YSL LDs, whereas the $mttp^{stl/stl}$, $mttp^{c655/c655}$ and trans-heterozygous $mttp^{stl/c655}$ embryos
239 accumulate substantial numbers of cytoplasmic LDs (Figure 2B). LDs in $mttp^{stl/stl}$ mutants are
240 more numerous and more uniform in size, whereas the $mttp^{c655/c655}$ mutants often had very large
241 LDs in addition to small droplets (Figure 2C). As a result, the number of LDs per area of the
242 YSL is reduced in the $mttp^{c655/c655}$ mutants compared to $mttp^{stl/stl}$ mutants (Figure 2D). The trans-
243 heterozygous fish had LDs that were more similar in size to the $mttp^{stl/stl}$ mutants and had a trend
244 toward fewer lipid droplets per YSL area, although this was not significant.
245

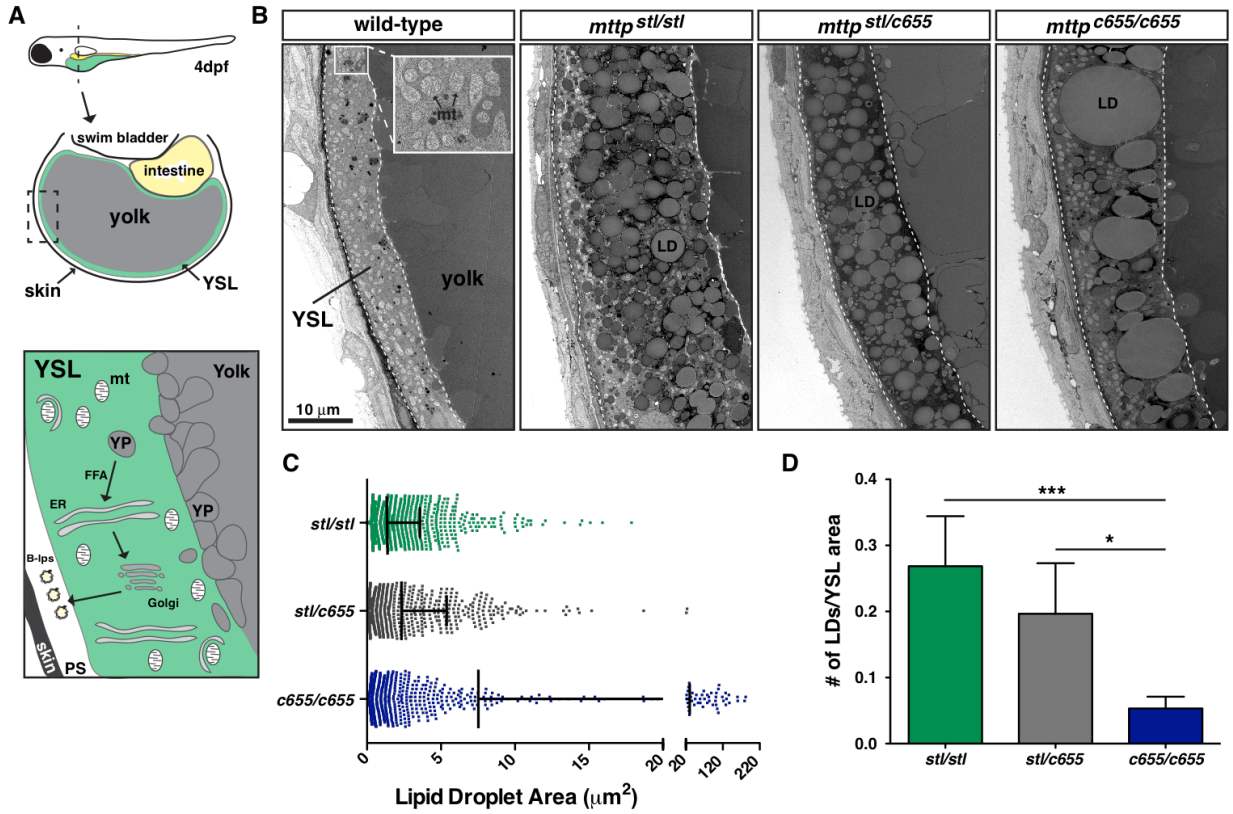

Figure 2: The opaque yolk phenotype results from the accumulation of aberrant cytoplasmic lipid droplets in the yolk syncytial layer. (A) (Top) Cartoon depicting the cross-sectional view of a 4-dpf zebrafish embryo. The yolk syncytial layer (YSL) surrounds the yolk mass and serves as the embryonic digestive organ. The dashed box indicates the view expanded in the bottom panel and in panel B. (Bottom) Stored yolk lipids undergo lipolysis in yolk platelets (YP), presumably releasing free fatty acids into the YSL. These fatty acids are re-esterified in the ER bilayer to form triglycerides, phospholipids, and cholesterol esters. The lipids are packaged into ApoB-containing lipoproteins in the ER with the help of MTP and are further processed in the Golgi before being secreted into the perivitelline space (PS) and then circulation. (B) Representative transmission electron micrographs of the yolk and YSL from wild-type and *mttp* mutants; dashed lines delineate the YSL region, mt = mitochondria, scale = 10 μm. (C) Quantification of lipid droplet size in *mttp* mutants, n ≥ 700 lipid droplets in 2 fish per genotype; mean +/- SD. (D) Quantification of the number of lipid droplets per YSL area, n = 7-9 YSL regions per genotype (3–5 regions per fish, 2 fish per genotype); mean +/- SD, Kruskall-Wallis with Dunn's Multiple Comparison test, vs. $mttp^{c655/c655}$ * $p < 0.05$, *** $p < 0.001$.

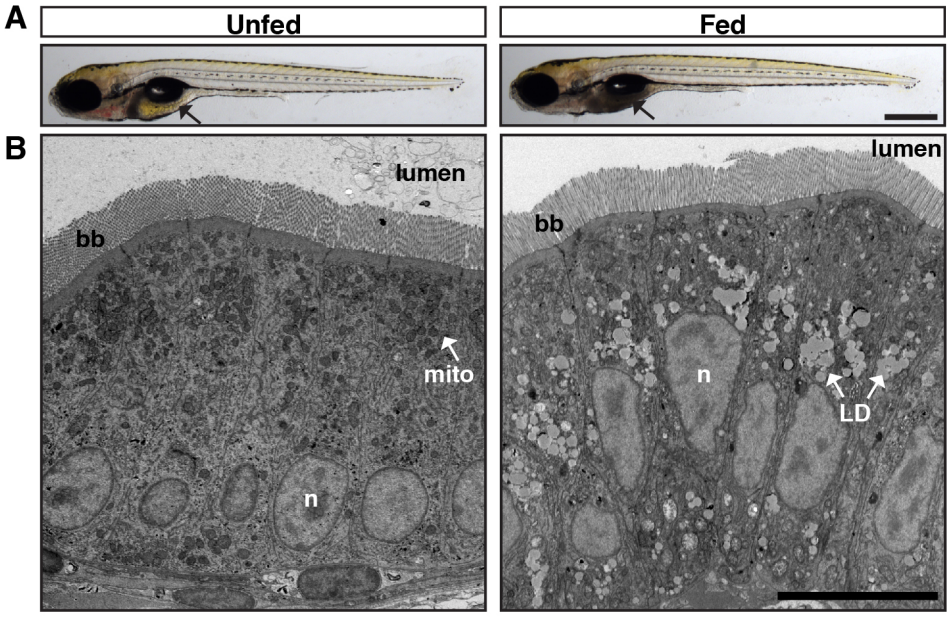

263
264
265 **Figure 2 – figure supplement 1: Lipid droplets block light transmission through the larval**
266 **intestine.** (A) Wild-type fish at 6 dpf were fed a high-fat meal for 1h as described previously
267 (Otis and Farber, 2016). Unfed fish have translucent intestines (black arrow, left) when imaged
268 with transmitted light, whereas fed fish have opaque intestines (black arrow, right). Scale = 500
269 μM. (B) Electron microscopy following a 1 h high-fat feed reveals an accumulation of
270 cytoplasmic lipid droplets in the intestinal enterocytes. By scattering light and blocking light
271 transmission through the intestine, the accumulation of cytoplasmic lipid droplets causes the
272 intestine to appear opaque. Nucleus (n), mitochondria (mito), brush border (bb), lipid droplet
273 (LD). Scale = 10 μM.
274
275
276 ***The stl and c655 mutations have differential effects on adult size and steatosis.*** Patients
277 with Abetalipoproteinemia often present in infancy with growth retardation, diarrhea, fat
278 malabsorption, and failure to thrive (reviewed in (Lee and Hegele, 2014)), and whole body
279 deficiency of MTP in a murine model is embryonic lethal (Raabe et al., 1998). In agreement
280 with the mouse phenotype, in the original characterization of the zebrafish *mttp*$^{stl/stl}$ phenotype it
281 was noted that the fish did not survive past 6 days post fertilization (dpf)(Avraham-Davidi et al.,
282 2012). Therefore, we were surprised to find that some of the *stl* mutants were able to survive
283 past larval stages. While these fish are generally much smaller in length and mass (Figure
284 3A,B) and their viability is reduced relative to their siblings (expected 25%, observed 3.8%

285 [5/131 fish] at 7.5 months), some of these fish have survived to be at least 18 months old.
286 Survival rates are better when the mutants are reared separately and are not competing with
287 siblings for food. Although these fish can reproduce, this is rare. In contrast, the *mttp*$^{c655/c655}$
288 mutants do not exhibit reduced viability and we did not find any reduction in size or fertility of the
289 *c655* mutants compared with siblings (Figure 3A,B). No difference in length or mass was noted
290 in fish trans-heterozygous for *mttp*$^{stl/c655}$ (Figure 3A,B).
291

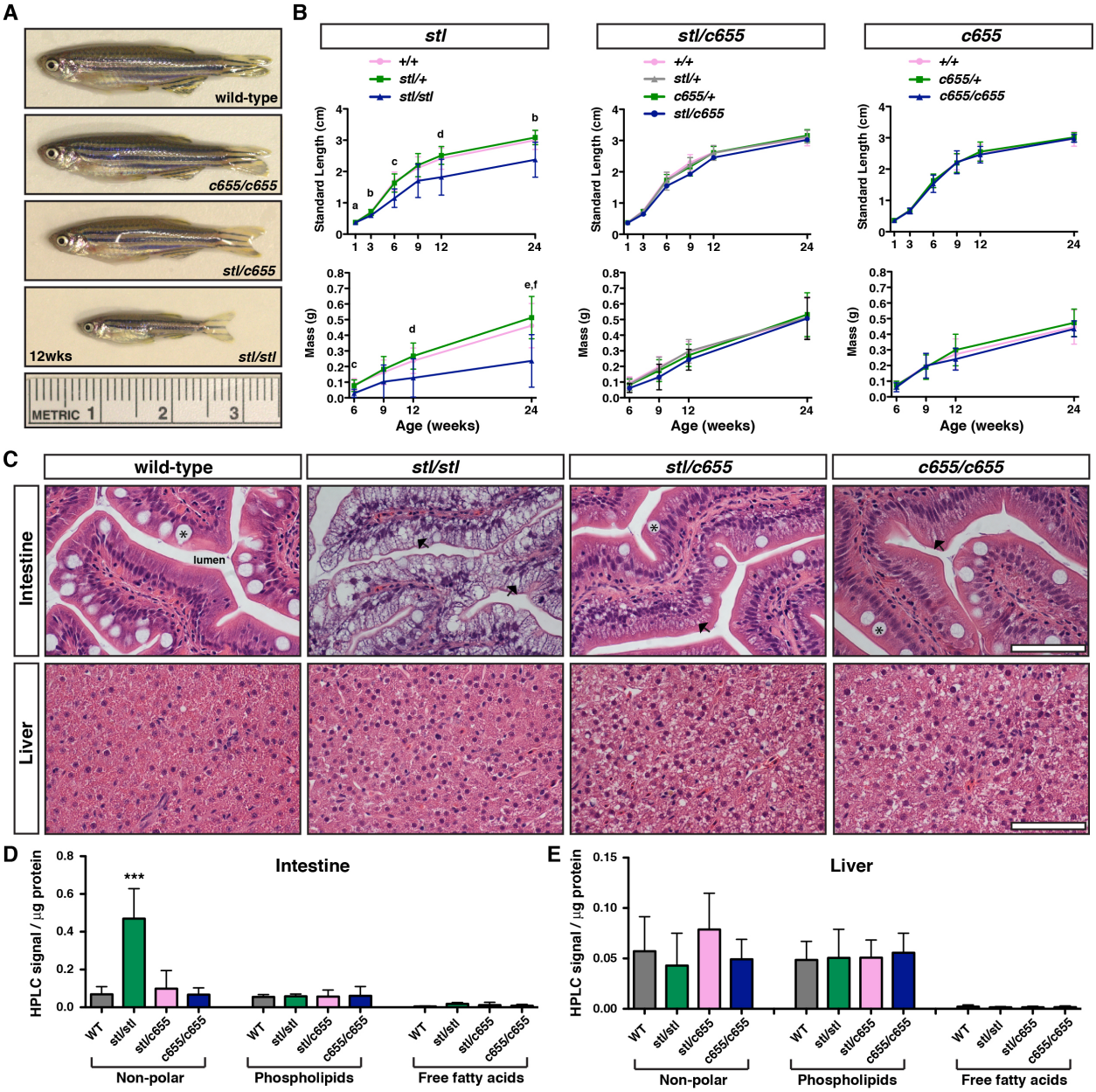

292
293

Figure 3: The *stl* and *c655 mttp* mutations have differential effects on the growth and accumulation of lipid in intestine. (A) Representative images of WT and *mttp* mutant fish at 12 weeks of age. (B) Developmental time-course of standard length and mass measurements of *mttp* mutant fish and siblings. Results are representative of pooled data from two independent experiments, n = 7–80 fish/genotype/time-point, mean +/- SD. Significance was determined with a Robust ANOVA and Games-Howell post-hoc tests were used to make pair-wise comparisons at each time point. Using a Bonferroni correction, p-values were adjusted to control for multiple comparisons (6 length or 4 mass comparisons), a: *stl/+* vs. *stl/stl*, $p < 0.01$; b: *+/+* vs. *stl/stl* and *stl/+* vs. *stl/stl*, $p < 0.05$; c: *+/+* vs. *stl/stl* and *stl/+* vs. *stl/stl*, $p < 0.001$; d: *stl/+* vs. *stl/stl*, $p < 0.05$; e: *+/+* vs. *stl/stl*, $p < 0.01$; f: *stl/+* vs. *stl/stl*, $p < 0.001$. (C) Representative images of H&E stained intestine and liver from adult WT and *mttp* mutant fish (7.5 months), scale = 50 μm, * indicate goblet cell, arrows indicate representative lipid accumulation in enterocytes. (D & E) Quantification of non-polar lipids, phospholipids, and free fatty acids in intestine and liver tissue using high-performance liquid chromatography; n = 5–6 fish per genotype, mean +/- SD, One-way ANOVA with Bonferroni post-hoc tests were performed separately for each lipid class; *** $p < 0.001$ *stl/stl* vs. all other genotypes.

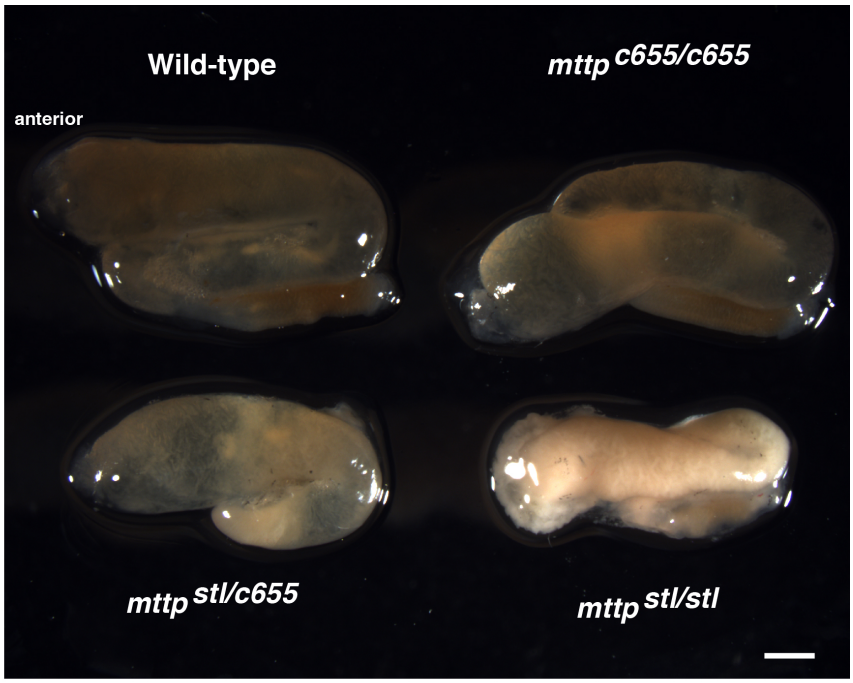

314 **Figure 3 – figure supplement 1: Significant lipid accumulation in the intestine of *stl/stl***
315 **but not in *c655/c655* mutants.** Representative images of isolated intestines from adult WT
316 and *mttp* mutant fish (7.5 months), scale = 1 mm.
317
318
319 To assess why the *mttp*$^{stl/stl}$ mutants, but not the *mttp*$^{c655/c655}$ mutants, have defects in growth, we
320 examined whether the mutations have differential effects on fat malabsorption. H&E staining of
321 intestinal tissue from fasted adults revealed gross accumulation of lipid in the cytoplasm of
322 enterocytes in the *mttp*$^{stl/stl}$ fish (Figure 3C, Figure 3 – figure supplement 1). The *mttp*$^{c655/c655}$
323 mutants were largely protected from this abnormal lipid retention. While the trans-heterozygous
324 fish exhibited more visible lipid retention than either wild-type or *mttp*$^{c655/c655}$ fish, this was not as
325 profound as in the *mttp*$^{stl/stl}$ fish. Retention of non-polar lipid (TG and cholesterol ester),
326 phospholipid, and free fatty acids in the intestine were also quantified using HPLC and the
327 *mttp*$^{stl/stl}$ mutants contain ~7 times more neutral lipid than *c655* mutants (Figure 3D). This data
328 suggests the growth defects in *mttp*$^{stl/stl}$ mutants result from defects in dietary lipid absorption in
329 the intestine.
330
331 Besides accumulating lipids in the intestine, Abetaliporoteinemia patients sometimes develop
332 hepatic steatosis (reviewed in (Lee and Hegele, 2014)). Similarly, hepatocyte-specific deficiency
333 of MTTP in mice causes TG and cholesterol to accumulate in the liver (Khatun et al., 2012;
334 Raabe et al., 1999). Therefore, we hypothesized that the adult zebrafish *mttp* mutants would
335 also exhibit liver steatosis. However, mutants were not different than wild-type (Figure 3C,D).
336 Moreover, there was no significant difference in measured lipids in the livers of the different fish
337 (Figure 3E). While we were surprised that the *mttp*$^{stl/stl}$ mutants had very little accumulation of
338 lipid in their livers, this is in agreement with findings that combined intestinal and liver deficiency
339 of Mttp in mice results in accumulation of TG in the intestine, but not in the liver (Iqbal et al.,
340 2015).
341
342 ***Mttp mutations reduce the size and number of ApoB-containing lipoproteins in vivo.*** To
343 understand how the *mttp* mutations affect the production and size of B-lps during embryonic
344 development, we crossed the *mttp*^{stl} and *mttp*^{c655} mutations into our LipoGlo reporter line
345 (Thierer et al., In Press). These fish express an in-frame fusion of the engineered luciferase
346 reporter Nanoluc at the C-terminus of the Apolipoprotein Bb.1 gene (Figure 4A). Since ApoB is

347 an obligate structural component of B-lps with only one copy per lipoprotein particle (Elovson et
348 al., 1988), the relative number of tagged lipoprotein particles can be quantified using the Nano-
349 Glo assay in extracts from transgenic fish (Thierer et al., In Press). B-lp levels were measured
350 in whole fish lysate throughout embryonic development from 2–6 dpf. During this time, the fish
351 are relying solely on yolk lipids and the ApoB quantity measurements reflect lipoprotein particles
352 in the secretory pathway in the YSL, in the circulation, and in cells prior to degradation of
353 endocytosed lipoproteins. Wild-type embryos exhibit an increase in B-lp particle number from
354 2–3 dpf as yolk lipid is packaged into lipoproteins, and then numbers decline as the yolk is
355 depleted and the lipids in the lipoproteins are taken up by target tissues and lipoprotein particles
356 are degraded (Figure 4B). The *mttp*$^{c655/c655}$ embryos have the same relative number of ApoB
357 particles as wild-type embryos at 2 dpf, but from 3-6 dpf the numbers of particles never reach
358 wild-type levels and decline more rapidly. In contrast, *mttp*$^{stl/stl}$ embryos have profound defects
359 in B-lp production, since amount of ApoB is significantly lower than wild-type siblings at 2 dpf
360 (Figure 4B) (Thierer et al., In Press).
361
362

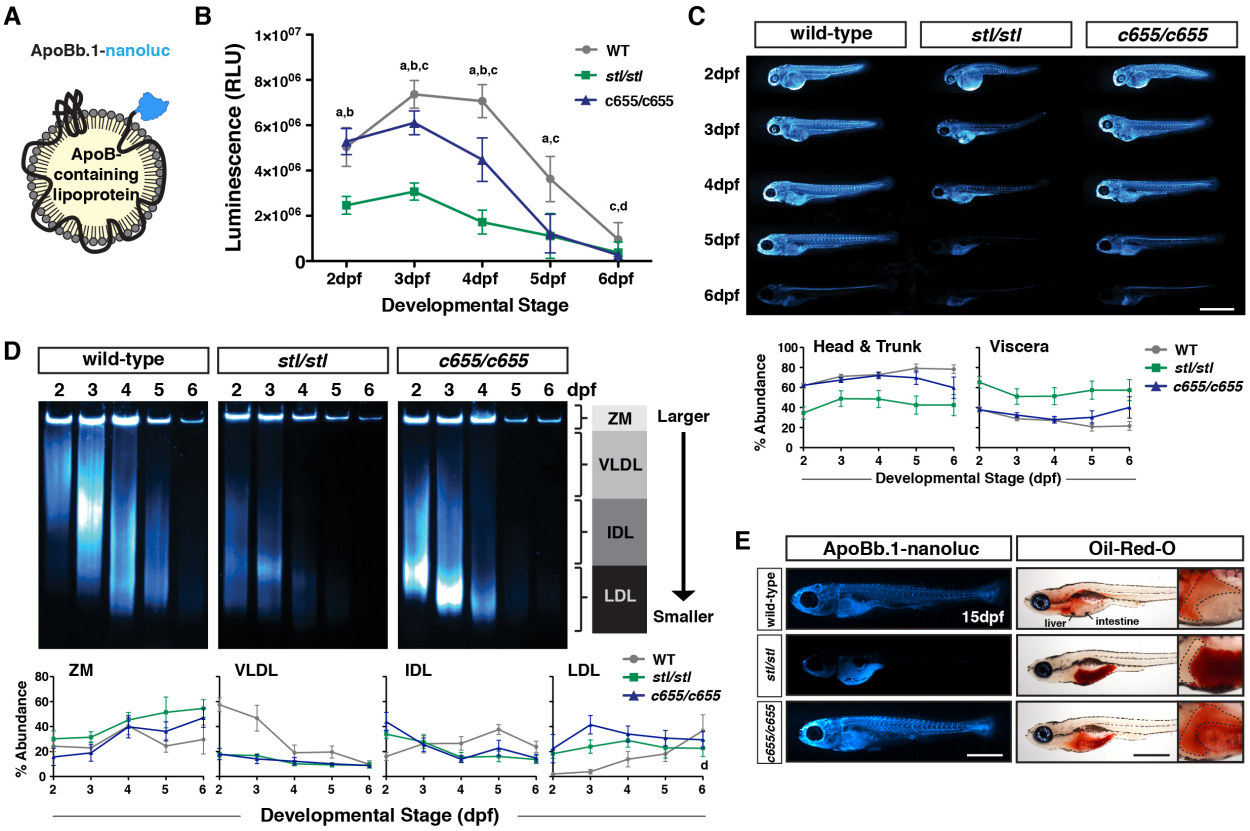

363
364

365 **Figure 4: The *stl* and *c655* mttp mutations have differential effects on ApoB-containing**
366 **lipoprotein number, size and distribution *in vivo*.** (A) LipoGlo fish express the Nanoluc®
367 luciferase enzyme as a C-terminal fusion on ApoBb.1 as a result of TALEN-based genomic
368 engineering. (B) LipoGlo signal (RLU: relative luminescence units) in WT, *mttp*$^{stl/stl}$ and
369 *mttp*$^{c655/c655}$ fish throughout embryonic development (2–6 dpf). Results represent pooled data
370 from 3 independent experiments, n = 22–34 fish/genotype/time-point. Significance was
371 determined with a Robust ANOVA, Games-Howell post-hoc tests were performed to compare
372 genotypes at each day of development, and p-values were adjusted to control for multiple
373 comparisons, a = WT vs. *mttp*$^{stl/stl}$, $p<0.001$, b = *mttp*$^{c655/c655}$ vs. *mttp*$^{stl/stl}$, $p<0.001$, c = WT vs.
374 *mttp*$^{c655/c655}$, $p<0.001$, d = WT vs. *mttp*$^{stl/stl}$, $p<0.05$. (C) Representative whole-mount images of
375 B-lp localization using LipoGlo chemiluminescent microscopy in WT, *mttp*$^{stl/stl}$, and *mttp*$^{c655/c655}$
376 fish throughout development; scale = 1 mm. Graphs represent pooled data from 3 independent
377 experiments, n = 13–19 fish/genotype/time-point; *mttp*$^{stl/stl}$ had a significantly different ApoB
378 localization from WT and *c655/c655*, $p<0.001$, Robust ANOVA. Post-hoc analysis reveals
379 statistical differences at all developmental stages $p<0.05$–0.001 (Games-Howell). (D)
380 Representative LipoGlo PAGE gels and quantification of B-lp size distribution from whole
381 embryo lysates during development. B-lps are divided into four classes based on mobility,
382 including zero mobility (ZM), and three classes of serum B-lps (VLDL, IDL and LDL). Graphs
383 show subclass abundance for WT, *mttp*$^{stl/stl}$, and *mttp*$^{c655/c655}$ fish at each day of embryonic
384 development as described in (Thierer et al., In Press). Results represent pooled data from n = 9
385 samples/genotype/time-point; at each particle class size, there were statistically significant
386 differences between genotypes (Robust ANOVA, $p<0.001$). Games-Howell post-hoc analysis
387 revealed numerous differences between genotypes at each developmental stage, see figure
388 supplement 2. (E) Representative whole-mount images of LipoGlo microscopy and Oil Red O
389 imaging in 15-dpf embryos chow-fed for 10 days and fasted ~18hrs prior to fixation; scale = 1
390 mm. Livers (outlined) are magnified for clarity in insets on right. Results represent pooled data
391 from 3 independent experiments, n = 15 fish/genotype/time-point.
392
393
394 To assess the localization of the B-lps throughout the embryos during development, we fixed
395 the embryos expressing ApoBb.1-nanoluc and performed chemiluminescent whole-mount
396 imaging (Figure 4C). Wild-type and *mttp*$^{c655/c655}$ embryos exhibit a similar distribution pattern of
397 LipoGlo throughout 2–4 dpf, but consistent with the quantitative assay, the signal in the head

398 and trunk decline more rapidly in *mttp*$^{c655/c655}$ fish. By 6 dpf, both wild-type and *mttp*$^{c655/c655}$ fish
399 show an accumulation of ApoB in the liver and the spinal cord (Figure 4C) (Thierer et al., In
400 Press). The LipoGlo in the *mttp*$^{stl/stl}$ embryos shows a very different pattern, in that it is
401 predominantly localized to the YSL/viscera at all stages and is at very low levels throughout the
402 rest of the body (Figure 4C). This is consistent with the prolonged retention of the opaque yolk
403 phenotype (Figure 1 – figure supplement 3) and suggests that the *mttp*$^{stl/stl}$ mutants are more
404 defective at secreting B-lps from the yolk than the *mttp*$^{c655/c655}$ mutants.
405
406 To determine whether the *mttp* mutations alter the size distribution of B-lps, we performed
407 native polyacrylamide gel electrophoresis of larval homogenates expressing the LipoGlo
408 reporter. Following electrophoretic separation and chemiluminescent imaging of the gels, B-lps
409 were classified into four different classes based on their migration distance (zero mobility, very
410 low-density lipoproteins (VLDL), intermediate-density lipoproteins (IDL), or low-density
411 lipoproteins (LDL)(Thierer et al., In Press). During development, the pattern of B-lps in wild-type
412 embryos is initially defined by VLDL (2 dpf), but expands to include IDL and LDL by 3–4 dpf as
413 the VLDL particles produced by the YSL are lipolyzed by the body tissues (Figure 4D, Figure 4
414 – figure supplement 1, (Thierer et al., In Press)). By 5–6 dpf, the yolk is depleted and any
415 remaining small particles are degraded. In contrast, both *mttp*$^{stl/stl}$ and *mttp*$^{c655/c655}$ embryos
416 produce very few VLDL particles (Figure 4D, 2 dpf), and instead, produce predominantly IDL
417 and LDL-sized particles.
418

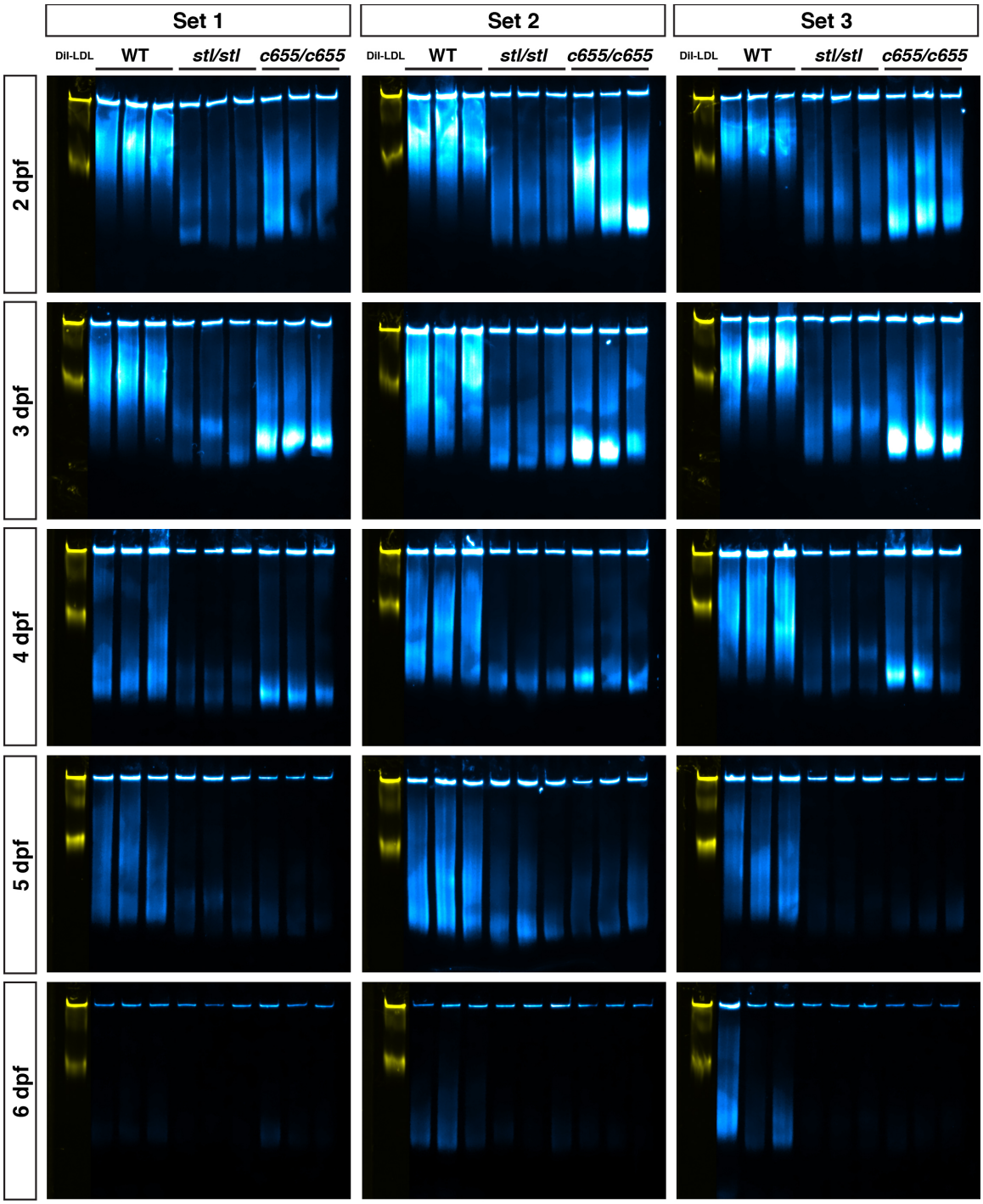

Figure 4 – figure supplement 1: LipoGlo lipoprotein gel primary data. Original gels corresponding to the data in Figure 4D. Each gel shows a composite image of the fluorescent DiI-LDL migration standard (yellow) and LipoGlo emission chemiluminescent exposure (blue) from WT, *mttp*$^{stl/stl}$ and *mttp*$^{c655/c655}$ fish. Gels were analyzed as detailed in (Thierer et al., In Press) and lipoprotein particles were binned into four classes based on migration relative to the

426 DiI-LDL standard, including zero mobility (ZM), and three classes of serum B-lps (VLDL, IDL
427 and LDL).
428
429 **Figure 4 – figure supplement 2:**

	Zero Mobility Band	VLDL Fraction	IDL Fraction	LDL Fraction
2 dpf				
WT vs. *stl/stl*	n.s.	p < 0.0005	p < 0.0005	p < 0.0005
WT vs. *c655/c655*	n.s.	p < 0.0005	p < 0.0005	p = 0.01
stl/stl vs. *c655/c655*	p = 0.005	n.s.	n.s.	
3 dpf				
WT vs. *stl/stl*	p = 0.015	p < 0.0005	n.s.	p < 0.0005
WT vs. *c655/c655*	n.s.	p < 0.0005	n.s.	p < 0.0005
stl/stl vs. *c655/c655*	p = 0.005	n.s.	n.s.	p < 0.0005
4 dpf				
WT vs. *stl/stl*	n.s.	p = 0.003	p = 0.005	P < 0.005
WT vs. *c655/c655*	n.s.	n.s.	p < 0.0005	P < 0.005
stl/stl vs. *c655/c655*	n.s.	n.s.	n.s.	n.s
5 dpf				
WT vs. *stl/stl*	p < 0.0005	p < 0.0005	p < 0.0005	n.s.
WT vs. *c655/c655*	p = 0.025	p = 0.005	p < 0.0005	p = 0.005
stl/stl vs. *c655/c655*	n.s.	n.s.	n.s	n.s.
6 dpf				
WT vs. *stl/stl*	p < 0.0005	n.s.	p < 0.0005	n.s.
WT vs. *c655/c655*	p = 0.03	n.s.	p = 0.005	n.s.
stl/stl vs. *c655/c655*	n.s.	n.s.	n.s.	n.s.

430 n.s. = not significant
431
432
433 Taken together, the LipoGlo data from embryos indicates that the *mttp*$^{stl/stl}$ and *mttp*$^{c655/c655}$
434 embryos are producing and secreting fewer, smaller B-lps from the yolk, although the effect is
435 more severe in *stl* mutants. Given the gross accumulation of lipid in the intestines of the adult
436 *mttp*$^{stl/stl}$ mutants, compared to the *mttp*$^{c655/c655}$ fish (Figure 3C), we hypothesize that the *mttp*$^{stl/stl}$
437 mutants are also less effective at secreting chylomicrons from the enterocytes. To test this
438 hypothesis, we performed chemiluminescent imaging using the LipoGlo reporter in 15-dpf larvae
439 fed a chow diet for 10 days and then fasted overnight. Wild-type LipoGlo fish have abundant
440 ApoB throughout their circulation and tissues (73.1+/- 4.0% in head and trunk vs. 26.9 +/-4.0%
441 in viscera, mean +/- SD, n = 15 fish) (Figure 4E). The *mttp*$^{c655/c655}$ mutation does not prevent
442 secretion of ApoB to the body tissues (73.1 +/- 3.7% in head and trunk vs. 26.9 +/- 3.7% in
443 viscera). In contrast, the *mttp*$^{stl/stl}$ fish have abundant LipoGlo signal in their intestine, and much
444 less in other tissues compared to WT (41% +/- 11% in head and trunk vs. 59 +/- 11% in viscera,
445 p<0.001, Kruskall-Wallis & Dunn's Multiple Comparisons Test) (Figure 4E). In agreement,
446 staining the neutral lipid with Oil Red O indicates *mttp*$^{stl/stl}$ mutants retain substantial lipid in their

447 intestines, whereas *mttp*$^{c655/c655}$ mutant fish have less lipid remaining in their intestine, but do
448 accumulate some lipid in their livers (Figure 4E). This data argues that the *stl* mutation severely
449 reduces B-lp secretion, not only from the yolk, but also from the enterocytes, whereas the *c655*
450 mutation only mildly decreases ApoB secretion in both embryos and larvae.
451
452 ***The c655 mutation in zebrafish mttp disrupts the triglyceride transfer activity but not the***
453 ***phospholipid transfer activity of the MTP complex.*** The dissimilar phenotypes of *in vivo* B-lp
454 secretion between the *stl* and *c655* mutations suggest that the two mutations are differentially
455 affecting MTP function. To provide molecular explanations for the phenotypes observed in the
456 different zebrafish mutants and to dissect further how each of the mutations affects MTP
457 function, we used cell and *in-vitro*-based assays of MTP function. COS-7 cells expressing
458 human ApoB48 were co-transfected with either an empty vector (pcDNA3), or a vector
459 containing wild-type zebrafish *mttp*, *mttp-stl* or *mttp-c655*, all with C-terminal FLAG-tags. We
460 found that *stl* and *c655* expressing COS-7 cells have significantly reduced concentrations of
461 ApoB in the conditioned media compared to wild-type Mttp expressing cells (Figure 5A). ApoB
462 levels in the media of the *stl*-expressing cells were similar to cells transfected with empty vector,
463 indicating background secretion levels. The concentration of ApoB48 was significantly higher in
464 the media of *c655*-expressing COS-7 cells compared to the *stl*-expressing cells and cells
465 transfected with empty vector (Figure 5A). ApoB48 concentrations in the cell lysate of cells
466 expressing *stl* were significantly higher than wild-type Mttp and *c655*-expressing cells (Figure
467 5B). These data suggest that the *stl* mutation does not support ApoB48 secretion whereas the
468 *c655* mutation does support ApoB48 secretion, but with reduced efficacy compared to wild-type
469 Mttp.
470

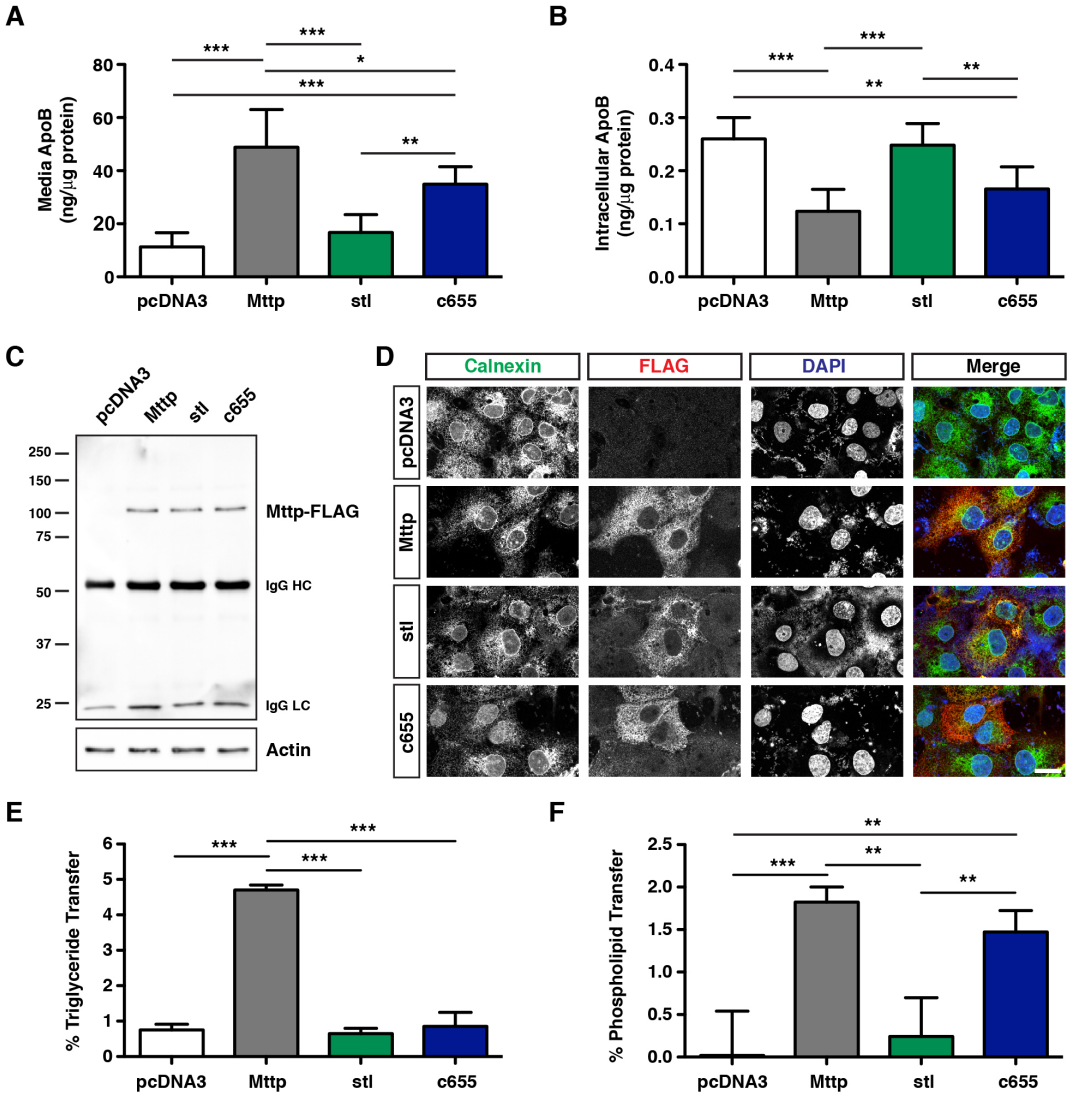

Figure 5: The *c655* mutation disrupts the triglyceride transfer activity, but not the phospholipid transfer activity of the zebrafish MTP complex. (A-B) COS-7 cells were first transfected with an expression vector for human apoB48 (5 μg), distributed equally in 6-well plates, and subsequently transfected with plasmids expressing either wild-type zebrafish *mttp*-FLAG, *mttp*^{stl}-FLAG, *mttp*^{c655}-FLAG, or empty vector (pcDNA3) (3 μg). After 72 h, ApoB48 was measured via ELISA in media (A) or in the cell (B). Data are representative of 7 independent experiments (each data point is the mean of 3 technical replicates), mean +/- SD, One-Way ANOVA with Bonferroni post-hoc tests, * $p<0.05$, ** $p<0.01$, *** $p<0.001$. (C) Cos-7 cells were transfected as described above and FLAG-tagged proteins were immunoprecipitated from cell lysates using anti-FLAG antibodies and eluted with FLAG peptides. Representative Western

484 blot on eluted fractions indicates equal concentrations of the various Mttp-FLAG proteins; actin
485 blot indicates equal loading of cell lysate. (D) Representative immunofluorescent staining using
486 anti-FLAG (red) and anti-Calnexin (green) antibodies in COS-7 cells expressing wild-type or
487 mutated *mttp*-FLAG constructs; scale = 25 μm. (E) COS-7 cells were transfected with plasmids
488 expressing pcDNA3, wild-type *mttp-FLAG*, or mutant *mttp*-FLAG constructs. Cells were lysed
489 and 60 μg of protein was used to measure the % triglyceride transfer of NBD-triolein from donor
490 to acceptor vesicles after 45 minutes; n = 3 (each n is the mean of three technical replicates
491 from independent experiments), mean +/- SD, One-way ANOVA with Bonferroni post-hoc tests,
492 *** $p<0.001$. (F) Wild-type and mutant Mttp proteins were purified using anti-FLAG antibodies
493 and used to measure the % transfer of NBD-labeled phosphoethanolamine triethylammonium
494 from donor to acceptor vesicles after 180 minutes; n = 3 (each n is the mean of 3 technical
495 replicates from independent experiments), mean +/- SD, randomized block ANOVA with
496 Bonferroni post-hoc tests, ***$p<0.001$.
497
498 To eliminate the possibility that the *stl* mutation did not support ApoB48 secretion due to low
499 expression, Mttp, *stl*, and *c655* were precipitated using anti-FLAG antibodies from cell lysates
500 and were subjected to Western blot analysis. We found that there was no difference in the
501 expression of wild-type Mttp and Mttp mutants in COS-7 cells (Figure 5C). Another reason for
502 the *stl* mutation to be deficient in supporting ApoB48 secretion could be due to protein mis-
503 localization. To check this, we immunostained Mttp-expressing COS-7 cells with anti-Calnexin
504 and anti-FLAG antibodies. Confocal imaging shows that the wild-type Mttp and both mutant
505 proteins were properly localized in the endoplasmic reticulum (Figure 5D). Additionally, the
506 percentage of cells expressing the FLAG-tagged proteins were similar among all groups (Mttp-
507 FLAG 37%, Mttp-*stl* 31%, Mttp-*c655* 41% transfection efficiency). These studies suggest that
508 *stl* and *c655* mutant Mttp proteins are expressed to similar levels and are in the ER, where
509 lipoprotein assembly occurs.
510
511 Next, we hypothesized that the *stl* mutant protein may not support ApoB48 secretion because it
512 might be defective in lipid transfer activity. Triglyceride transfer assays performed using cell
513 lysates showed that both of the mutant forms of Mttp (*stl* and *c655*) have significantly decreased
514 triglyceride transfer activity compared to wild-type zebrafish Mttp (Figure 5E, Figure 5 – figure
515 supplement 1a). The *stl* mutant form was also found to be defective in phospholipid transfer

516 activity compared to wild-type (Figure 5F, Figure 5 – figure supplement 1b). Contrary to this,
517 the *c655* mutant form had similar phospholipid transfer activity to wild-type Mttp (Figure 5F,
518 Figure 5 – figure supplement 1b). These data suggest that the *c655* mutation in *mttp* impairs
519 triglyceride transfer, but not phospholipid transfer activity. In contrast, the *stl* mutation is
520 defective in both transfer activities. These differences in lipid transfer activities between the *stl*
521 and *c655* mutations provide a biochemical explanation for their differential abilities to support
522 ApoB48 secretion and the different phenotypes observed in the fish.
523
524

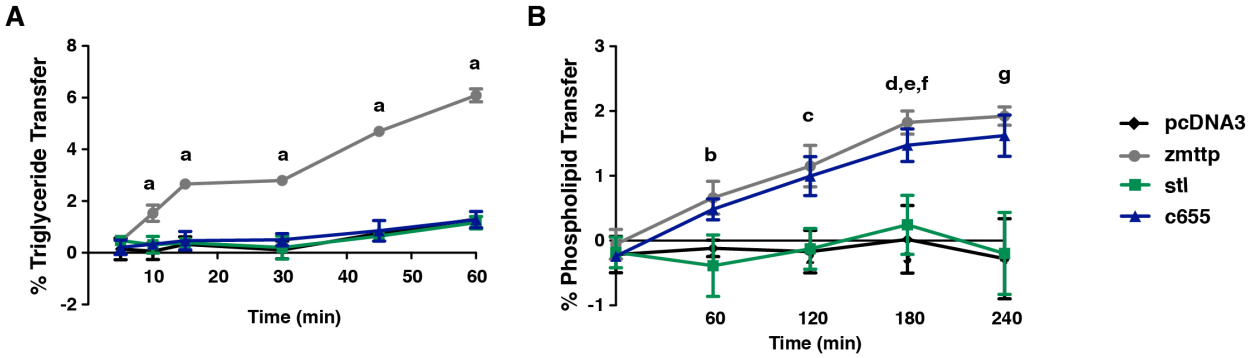

a; pcDNA3 vs. all others, p<0.001
b; zmttp vs. stl, p<0.05
c; pcDNA3 & stl vs. zmttp & c655, p<0.01
d; pcDNA3 vs. zmttp & c655, p<0.001
e; stl vs. zmttp, p<0.001
f: stl vs. c655, p<0.01
g; pcDNA3 & stl vs. zmttp & c655, p<0.001

525
526
527 **Figure 5 – figure supplement 1: Triglyceride and phospholipid transfer assay time-**
528 **course data.** Measurements for triglyceride (A) and phospholipid transfer (B) by zebrafish
529 *mttp*-FLAG and mutants over a time-course. The single time-points depicted in the bar graphs
530 of figures 5E & F, correspond to the 45 min & 180 min (triglyceride and phospholipid transfer,
531 respectively) time-points in the curves shown. For both, n = 3 (each n is the mean of 3 technical
532 replicates from independent experiments), mean +/- SD, Repeated Measures ANOVA with
533 Bonferroni post-hoc tests, significance as noted in figure.
534
535
536 ***An orthologous c655 mutation in human MTTP (G865V) also disrupts the triglyceride***
537 ***transfer activity but not phospholipid transfer activity.*** The M subunit of MTP shares
538 homology with lipovitellin, a lipid transfer protein in the yolk of oviparous animals (Banaszak et
539 al., 1991). Homology modeling with the crystal structure of lamprey lipovitellin (PDB ID:

540 1LSH)(Anderson et al., 1998; Raag et al., 1988; Thompson and Banaszak, 2002) predicts three
541 major structural domains in human MTTP: an N-terminal beta-barrel, a middle alpha-helical
542 domain, and a C-terminal domain composed of two beta-sheets that form a hydrophobic lipid-
543 binding cavity (Hussain et al., 2003a; Mann et al., 1999; Read et al., 2000). The amino acid
544 sequence of the zebrafish Mttp is 54% identical (72% similar) to that of human MTTP and the
545 predicted secondary and tertiary structures are highly conserved (Figure 6A).
546
547 The leucine residue mutated in the *stl* mutant fish (L475P) is conserved in human MTTP (L477)
548 and lies within a highly conserved stretch of amino acids located in the middle alpha-helical
549 domain of MTTP (Figure 6A). Analysis of mutations in patients with Abetalipoproteinemia has
550 shown that missense mutations in the alpha-helical domain often prevent lipid transfer activity
551 and result in loss of ApoB secretion (Reviewed in (Walsh and Hussain, 2017)). Therefore, it is
552 likely that the *stl* L475P mutation alters the structure of the lipid-binding cavity in a similar
553 manner to these patient mutations.
554
555 The glycine residue mutated in the C-terminus of *c655* mutants (G863V) is also conserved in
556 the human sequence (G865) (Figure 6A). Unfortunately, it is unknown where the G865 residue
557 is located in relation to the lipid-binding cavity because the C-terminal sequence of MTTP
558 diverges from that of lipovitellin, so it is not modeled in the predicted MTTP structure. However,
559 because the predicted tertiary structure of zebrafish Mttp is very similar to that of human MTTP
560 and the sequence in the C-terminus is highly conserved (Figure 6A), we hypothesized that
561 introduction of the *c655* mutation into the human MTTP protein would also cause loss of
562 triglyceride transfer, but retention of phospholipid transfer activity. To test this hypothesis, we
563 performed site-directed mutagenesis on the human *MTTP*-FLAG (hMTTP) plasmid and
564 assessed the function of the MTTP (G865V) mutant protein.
565

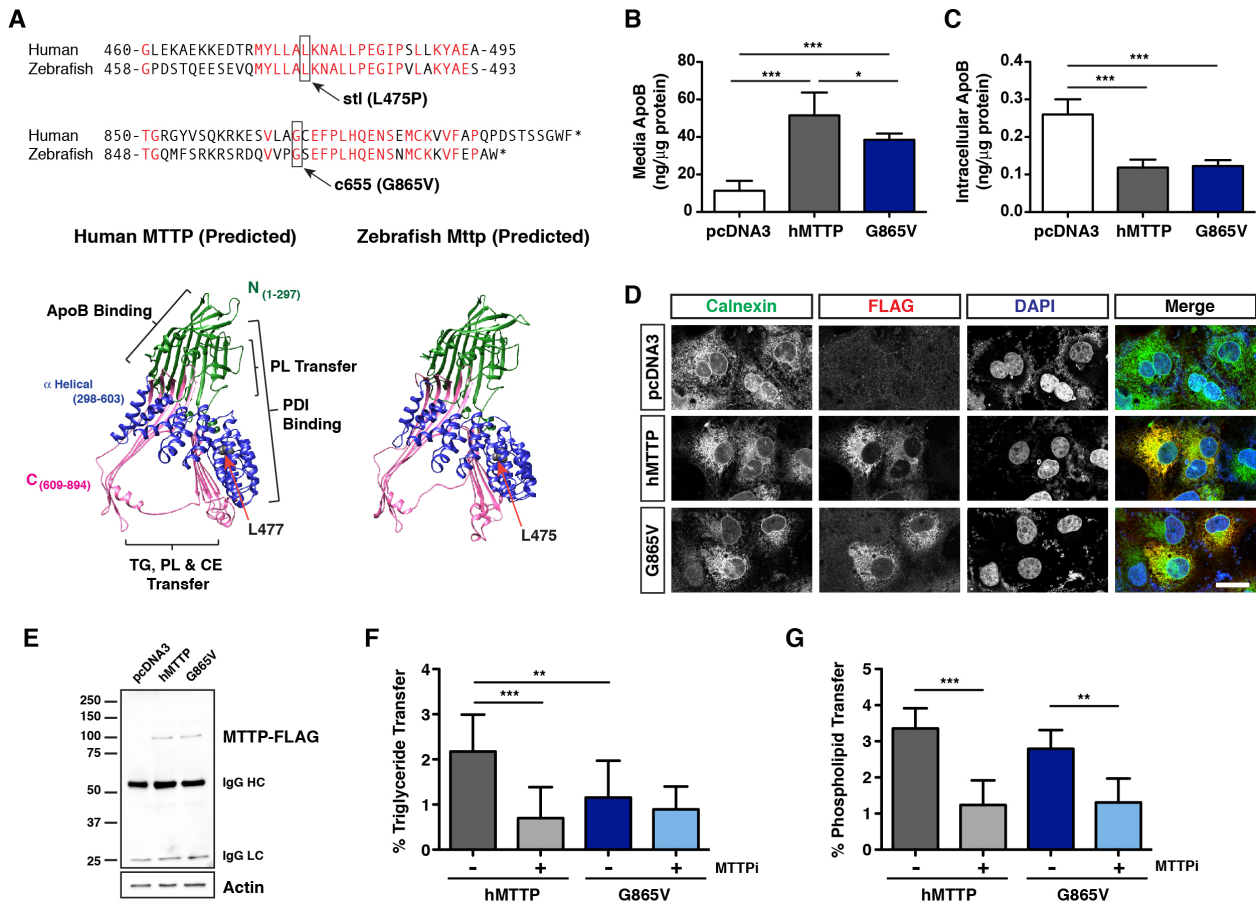

Figure 6: The *c655* mutation in human MTTP also disrupts the triglyceride transfer activity, but not the phospholipid transfer activity of the MTP complex. (A) Alignment of human and zebrafish Mttp amino acid sequences surrounding the *stl* or *c655* mutations. Ribbon diagrams of the predicted tertiary structures of human MTTP and zebrafish Mttp modeled using Phyre2 (Kelley et al., 2015) based on the lamprey lipovitellin structure (Anderson et al., 1998). The predicted phospholipid transfer sites in the N-terminal region (green) and the C-terminal region (pink, composed of two beta-sheets that form a hydrophobic lipid-binding pocket) are labeled. The location of the conserved human residue (L477) corresponding to the zebrafish *stl* (L475P) mutation is noted. The C-terminal region containing the *c655* mutation diverges from the lipovitellin structure and is not reliably modeled. (B,C) The *c655* mutation (G865V) was introduced into the human *MTTP*-FLAG plasmid. COS-7 cells were co-transfected with human ApoB48 and either wild-type human *MTTP*-FLAG, *MTTP*(G865V)-FLAG or empty pcDNA3 plasmids. After 72 h, apoB48 was measured via ELISA in media (B) or in the cell (C). Data are representative of 7 independent experiments (each data point is the mean of 3 technical replicates), pcDNA3 control data is re-graphed from figure 5A & 5B (data for 5A, 5B, 6B & 6C

583 were generated together); mean +/- SD, One-Way ANOVA with Bonferroni post-hoc tests, *
584 p<0.05, *** p<0.001. (D) Immunofluoresence in COS-7 cells expressing wild-type human
585 MTTP-FLAG or human MTTP(G865V)-FLAG using anti-FLAG (red) and anti-Calnexin (green)
586 antibodies; scale = 25 μm. (E) COS-7 cells were transfected and FLAG-tagged human MTTP
587 proteins were immunoprecipitated from cell lysates using anti-FLAG antibodies and eluted with
588 FLAG peptides. Representative Western blot on eluted fractions indicates equal concentrations
589 of the various MTTP-FLAG proteins; actin blot indicates equal loading of cell lysate. (F) COS-7
590 cells were transfected with plasmids expressing human wild-type or *MTTP*(G865V)-FLAG
591 constructs. Cells were lysed and 60 μg of protein was used to measure triglyceride transfer
592 activity in the presence or absence of the MTTP inhibitor lomitapide (1 μM)(% after 45 minutes);
593 n = 9 (3 measurements from each of 3 independent experiments), mean +/- SD, One-way
594 ANOVA with Bonferroni post-hoc tests, ** p<0.01, ***p<0.001). (G) Wild-type and mutant MTTP
595 proteins were purified using anti-FLAG antibodies and used to measure phospholipid transfer in
596 the presence or absence of lomitapide (1 μM) (180 minutes); n = 9 (3 measurements from each
597 of 3 independent experiments), mean +/- SD, randomized block ANOVA with Bonferroni post-
598 hoc tests, ** p<0.01, ***p<0.001.
599
600
601 COS-7 cells expressing the G865V mutant protein secreted slightly lower amounts (~75%) of
602 ApoB48 into the media compared to wild-type hMTTP, but this was significantly higher than the
603 background levels seen in cells transfected with the empty vector (pcDNA3) (Figure 6B).
604 ApoB48 concentrations in the cell lysate of cells expressing hMTTP and G865V mutant proteins
605 were similar (Figure 6C). These data suggest that the G865V mutation supports ApoB48
606 secretion albeit at lower efficiency. Attempts were made to explain the mechanisms for lower
607 efficiency in supporting ApoB secretion. Wild-type hMTTP-FLAG and G865V-FLAG were both
608 localized to the ER (Fig. 6D), transfection efficiency was similar (36% hMTTP, 35% G865V),
609 and the proteins were immunoprecipitated at similar levels from cell lysates (Figure 6E).
610 Triglyceride transfer assays with cell lysates of COS-7 cells expressing hMTTP-FLAG and
611 G865V-FLAG plasmids showed that the mutant G865V protein has significantly decreased
612 (~53%) triglyceride transfer activity compared to wild-type hMTTP, comparable to the activity
613 level of the WT hMTTP in the presence the MTTP inhibitor lomitapide (1 μM) (Figure 6F). In
614 contrast, the phospholipid transfer activity of hMTTP and G865V were not significantly different,

615 and the activity of both alleles were inhibited to equal extent by lomitapide (Figure 6G). These
616 data suggest that the *c655* mutation in both the zebrafish Mttp (G863V) and human MTTP
617 protein (G865V) results in significant loss of triglyceride transfer activity, but has no effect on
618 phospholipid transfer activity.
619
620
621
622 **DISCUSSION**
623
624 The characterization of the zebrafish *mttp c655* mutation provides the first evidence that the
625 triglyceride and phospholipid transfer functions of a vertebrate microsomal triglyceride transfer
626 protein can be dissociated and identifies the putative region responsible for triglyceride transfer
627 activity. Previous sequence comparisons of invertebrate and vertebrate orthologues of MTTP
628 strongly suggested that acquisition of triglyceride transfer activity during evolution was the result
629 of many changes in the lipid-binding cavity (Rava and Hussain, 2007), so it was unexpected that
630 one missense mutation in the C-terminus selectively eliminated triglyceride transfer activity.
631 Additionally, all of the characterized missense mutations from patients with
632 Abetalipoproteinemia cause MTP to be either absent or deficient in both phospholipid and
633 triglyceride transfer activities (Berthier et al., 2004; Di Filippo et al., 2012; Di Leo et al., 2005;
634 Khatun et al., 2013; Miller et al., 2014; Narcisi et al., 1995; Rehberg et al., 1996; Ricci et al.,
635 1995; Walsh et al., 2016; Walsh and Hussain, 2017; Walsh et al., 2015; Wang and Hegele,
636 2000).
637
638 While we do not know where the C-terminus is located in relation to the lipid-binding cavity
639 (Figure 6A), one of the Abetalipoproteinemia mutations (G865X) results in a C-terminal
640 truncation of 30 amino acids that prevents binding to PDI, thus resulting in loss of MTP protein
641 (Ricci et al., 1995). Subsequent analysis of constructs *in vitro* indicated that deletion of the last
642 20 amino acids (Δ20, S875X), or mutating the cysteine at position 878 (C878S), reduced the
643 expression of the protein to <15% of wild-type MTTP levels and abolished triglyceride transfer
644 activity (Narcisi et al., 1995). This cysteine residue is conserved in MTTP orthologues from
645 human to *C. elegans*, suggesting that it forms a disulfide bond essential for the tertiary structure
646 of the protein. The authors argue that the residual protein produced must be binding to PDI,
647 otherwise, no protein would be detected; however, it is unclear whether either of these mutated
648 proteins are still capable of transferring phospholipid (Narcisi et al., 1995). In contrast to these

649 mutations, the mutation of glycine to valine at position 865 in human MTTP (or 863 in zebrafish
650 mttp) does not reduce protein expression or alter the localization of MTTP in the ER of COS-7
651 cells (Figure 5D, 6D), indicating that the mutation does not interfere with PDI binding. This
652 suggests that the proposed disulfide bond is intact and that the G865V mutation may be more
653 directly affecting lipid transfer. Our data show that this mutation lacks the ability to transfer
654 triglycerides *in vitro*, but it is unclear whether the mutation also prevents binding of triglyceride in
655 the lipid-binding cavity. Perhaps binding can still occur, which would be consistent with the
656 evolutionary data, and maybe the C-terminus is necessary for transfer activity. Analyses of
657 Drosophila, zebrafish, or human MTTP chimeric proteins may help test this hypothesis in the
658 future. Additionally, in order to better understand how the *c655* mutation specifically inhibits
659 triglyceride transfer, a crystal structure including the C-terminus will likely be necessary.
660
661 The production of B-lps in the ER of the intestine and liver is thought to occur in two steps. In
662 the first step, MTP transfers lipids to ApoB as it is translated to form small primordial particles.
663 In the second step, it has been suggested that fusion of ApoB-free lipid droplets in the lumen of
664 the ER fuse to expand the lipoprotein core ("core expansion") (Alexander et al., 1976; Boren et
665 al., 1994; Hamilton et al., 1998; Wang et al., 1997). There is evidence to suggest that MTP is
666 also responsible for producing these ER-lumenal lipid droplets (Kulinski et al., 2002). Using our
667 LipoGlo assays, we have shown that the *c655* mutant fish produce small, homogenous,
668 particles, whereas the wild-type embryos form VLDL-sized lipoproteins in the YSL at 2–3 dpf
669 (Figure 4D). We have made similar observations in liver-specific *Mttp* KO mice expressing
670 Drosophila *Mttp*, which has robust phospholipid transfer activity, but is deficient in triglyceride
671 transfer (Khatun et al., 2012). Expression of fly Mttp resulted only in production of small B-lps,
672 but human MTTP rescued the particle size (Khatun et al., 2012). Therefore, the phospholipid
673 transfer activity of MTP may be crucial in the generation of the small homogenous particles
674 representative of the first step of lipoprotein assembly, whereas triglyceride transfer might be
675 primarily responsible for core expansion.
676
677 Although the effect of the *c655* mutation on the molecular function of the protein was
678 unexpected, the lack of intestinal or hepatic steatosis is also consistent with our previous data
679 with Drosophila Mttp expression in the livers of liver-specific Mttp-null mice. The phospholipid-
680 rich high-density B-lps produced by the fly Mttp in hepatocytes partially restore plasma lipid
681 levels and reduce liver steatosis (Khatun et al., 2012). Similarly, transfer of phospholipid and

682 production of small B-lps in the *c655* mutant fish is not only sufficient for moving lipid from the
683 liver, but is also capable of moving enough dietary lipid and fat-soluble vitamins from the
684 intestine to prevent intestinal steatosis and support normal growth (Figure 3,4). Furthermore,
685 retention of phospholipid transfer may also improve the health of the fish in ways that are
686 independent of lipoprotein production. For example, MTP-dependent phospholipid transfer has
687 been shown to be important for biogenesis and cell surface expression of CD1d and possibly
688 other lipid-antigen-presenting molecules (Dougan et al., 2005).
689
690 In contrast to the health and viability of *c655* mutants, the *stl* mutant fish that survive have gross
691 lipid accumulation in their intestine and severe growth defects (Figure 3,4), which is reminiscent
692 of patients with Abetalipoproteinemia. The mutant protein localizes normally to the ER, but is
693 deficient in triglyceride transfer, phospholipid transfer, and ApoB secretion (Figure 5). In the
694 predicted model of the tertiary structure of Mttp, this mutation is located in the middle alpha-
695 helical domain, not facing the lipid-binding cavity. The location and characterization of this
696 mutation is very similar to that of the described Y528H and S590I Abetalipoproteinemia
697 mutations, and it is likely that all three mutations prevent lipid transfer by altering the tertiary
698 structure of the M subunit (Khatun et al., 2013; Miller et al., 2014).
699
700 Counter to the original characterization of *stl* mutants (Avraham-Davidi et al., 2012), we show
701 that the *stl* mutants can survive to adulthood, especially when they are not competing with
702 siblings for resources. We hypothesize that during the maintenance of this mutant line since its
703 original characterization, a modifier has been eliminated that, when present in the *stl*
704 background, was incompatible with life. In support of this hypothesis, the excessive sprouting
705 angiogenesis defect for which the *stalactite* mutation was named (Avraham-Davidi et al., 2012),
706 was also not as severe as originally described (Supplementary Figure S1). Whether the
707 proposed modifier directly affects the secretion of B-lps, or some other aspect of development,
708 is currently unclear. While the *stl* mutation severely decreases B-lp number and particle size
709 (Figure 4D), some ApoB is still noted in the body of the $mttp^{stl/stl}$ embryos and larvae (Figure 4C,
710 4E). This suggests that there is enough transport of necessary lipids and fat-soluble vitamins by
711 the small numbers of B-lps produced by the YSL and intestine to support development.
712

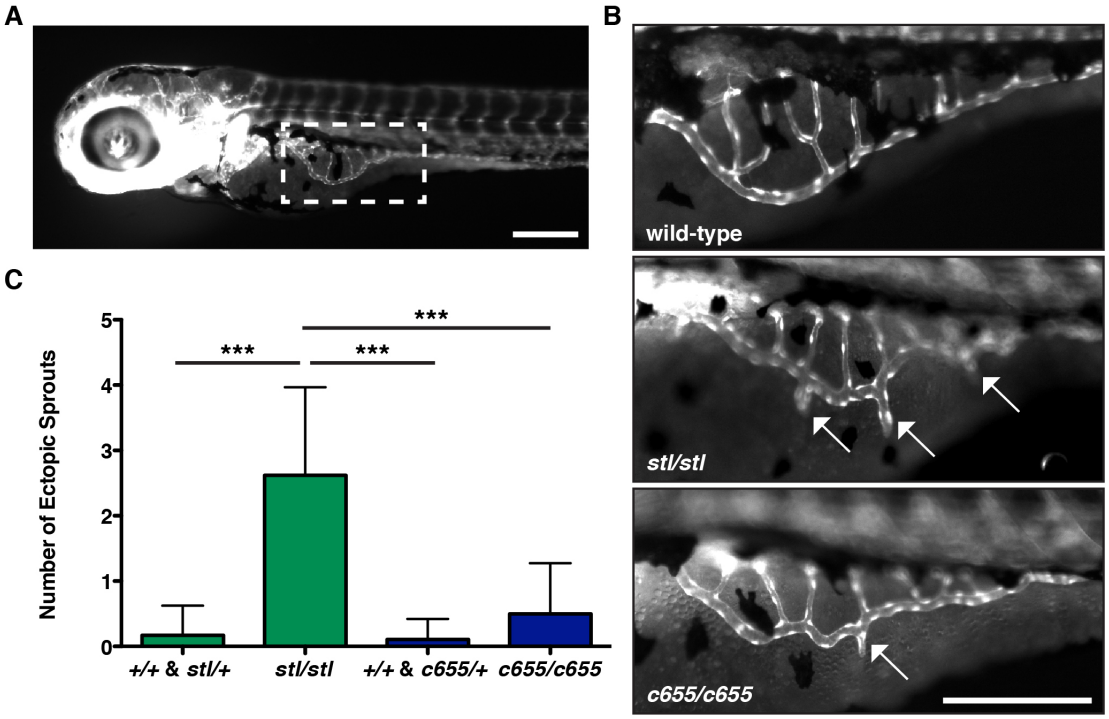

713
714 **Figure S1: *c655/c655* embryos exhibit fewer ectopic angiogenic segments extending**
715 **from the subintestinal vessels than *stl/stl* embryos.** (A) The developing vasculature is
716 visualized in the *Tg(fli:eGFP)*^{y1} transgenic zebrafish line (Lawson and Weinstein, 2002). The
717 subintestinal vessels (boxed region) grow bilaterally onto the dorsolateral surface of the yolk
718 sac. Scale = 200 μM. (B) Representative wide-field images of *Tg(fli:eGFP)*^{y1} in wild-type,
719 *mttp*$^{stl/stl}$ or *mttp*$^{c655/c655}$ embryos at 3.5 dpf. Ectopic sprouts extending ventrally from the
720 subintestinal vein are more common in *mttp*$^{stl/stl}$ mutant embryos than in *mttp*$^{c655/c655}$ mutant
721 embryos. Scale = 200 μM. (C) Quantification of the average number of ectopic sprouts in *mttp*
722 mutants and siblings on 3.5 dpf. Results represent pooled data from 3 independent
723 experiments, n = 28-36 total embryos/genotype group; mean +/- SD, Kruskall-Wallis with Dunn's
724 Multiple Comparison test, *** $p<0.001$.
725
726
727 The *c655* mutants were initially identified due to the abnormal opaque appearance of their yolks,
728 which is also a component of the *stl* mutant phenotype (Figure 1). We show that this opacity is
729 due to the abnormal accumulation of lipid droplets in the yolk syncytial layer (Figure 2). As the
730 lipids are liberated from the yolk, they are rapidly re-esterified to triglyceride and phospholipid
731 and packaged into B-lps in the endoplasmic reticulum of the YSL. Because the *mttp* mutant fish
732 are defective at producing (*stl*) and/or expanding (*c655*) B-lps, the re-esterified lipids are

733 packaged instead into cytoplasmic lipid droplets. In contrast, cytoplasmic lipid droplets are only
734 very rarely noted in the YSL of wild-type embryos, suggesting that the rate of yolk lipid break-
735 down and the rate of B-lp production and secretion from the YSL are exquisitely coupled. We
736 also noted that the size range of the cytoplasmic lipid droplets in the YSL of the *c655* mutants
737 was much larger than in the *stl* mutants, with some LDs reaching 180 μm^2. As the surface area-
738 to-volume ratio decreases with increasing size spheres, the larger lipid droplets store more
739 neutral lipid relative to the surface of the phospholipid coat. Because the *c655* mutants can
740 transfer phospholipid to ApoB and secrete greater numbers of small dense B-lps than *stl*
741 mutants, we hypothesize the retained neutral lipid is stored in larger lipid droplets because the
742 phospholipid is being secreted and less available to coat lipid droplets. However, it is unclear
743 whether the larger LDs form due to local production of triglycerides and cholesterol esters
744 directly on their surface, or due to lipid droplet fusion, or both mechanisms (reviewed in
745 (Olzmann and Carvalho, 2019; Walther et al., 2017)). The differences in the concentration and
746 size of LDs between the mutants may result in differential effects on the degree of light
747 scattering, which could explain the differences in opacity noted between mutants (Figure 1 –
748 figure supplement 3).
749
750 None of the missense mutations identified in patients with Abetalipoproteinemia have been
751 found to dissociate the lipid transfer activities of MTP (reviewed in (Walsh and Hussain, 2017)).
752 However, given that the adult *c655* mutant zebrafish are indistinguishable from wild-type
753 siblings, it is entirely possible that humans carrying a missense mutation that results in retention
754 of phospholipid transfer exist in the population. While these people would likely have low
755 plasma triglycerides, we would expect transport of fat-soluble vitamins to be normal. A thorough
756 search of publicly available large human GWAS databases (Global BioBank Engine, T2D
757 Knowledge Portal, GTEx Portal) did not reveal any coding variants near G865 other than the
758 G865X mutation discussed above. However, since one copy of wild-type MTTP is sufficient to
759 prevent fat malabsorption when faced with an oral fat load (Di Filippo et al., 2019), individuals
760 heterozygous for a mutation similar to *c655* may not present with any changes in plasma lipid
761 profiles.
762
763 Abnormally elevated levels of ApoB-containing lipoproteins and remnants promote
764 atherosclerosis, the leading cause of death in the United States (CDC, 2018). Inhibition of MTP
765 has long been considered a possible therapeutic target for lowering disease risk by inhibiting the

766 production of VLDL and chylomicrons (Jamil et al., 1996; Wetterau et al., 1998)(for review see
767 (Hussain and Bakillah, 2008; Walsh and Hussain, 2017)). Currently, the only MTP inhibitor
768 approved for use in patients is lomitapide (Juxtapid®), which inhibits triglyceride and
769 phospholipid transfer and reduces ApoB secretion (Robl et al., 2001)(Figure 6F,G). While this
770 drug effectively reduces LDL cholesterol, total cholesterol, and plasma ApoB levels, it is only
771 approved for patients with homozygous familial hypercholesterolemia, whose plasma
772 cholesterol and triglyceride levels are up to four times the normal levels resulting in premature
773 cardiovascular disease (Cuchel et al., 2014; Cuchel et al., 2013; FDA, 2012). While lomitapide
774 effectively lowers circulating lipid levels and reduces cardiovascular disease risk in these
775 patients, side effects include fat accumulation in the liver and adverse gastrointestinal events
776 including reflux, indigestion, abdominal pain, constipation, and diarrhea (Blom et al., 2017;
777 Cuchel et al., 2007; Cuchel et al., 2013).
778
779 The lack of intestinal and hepatic steatosis in the *c655* mutant fish suggests that an MTP
780 inhibitor that selectively targets triglyceride transfer activity could potentially lower plasma lipids
781 while preventing these gastrointestinal and liver side effects. This would not only improve the
782 quality of life for patients currently taking lomitapide, but may also expand MTP inhibitor use to
783 patients other than those with familial hypercholesterolemia. While one of the original MTP
784 inhibitors discovered, BMS-200150, was very effective at inhibiting triglyceride transfer, but less
785 effective (~30%) at inhibiting phospholipid transfer in vitro (Jamil et al., 1996), later studies on
786 purified MTP protein indicated the compound inhibits transfer of both lipid classes (Rava et al.,
787 2006) and that it was not effective in animal models (Wetterau et al., 1998). Now that we
788 appreciate that the triglyceride and phospholipid transfer functions of MTTP can be dissociated,
789 we argue that it may be worth re-evaluating the phospholipid transfer activity of any previously
790 identified compounds that inhibited triglyceride transfer activity of MTP, but failed to inhibit ApoB
791 secretion *in vitro*. Perhaps new compounds could be specifically designed to target the C-
792 terminal region of MTTP, although this will likely require a crystal structure of the MTP complex.
793
794 However, before a selective triglyceride transfer inhibitor could be considered as a therapeutic
795 for a wide range of patients with hyperlipidemia, it will be important to determine whether the
796 small lipoprotein particles produced by selective inhibition of triglyceride transfer are not
797 atherogenic. Small dense LDL has been found to have greater potential for causing
798 atherosclerosis than larger LDL sub-fractions and is a better predictor of cardiovascular disease

799 than total LDL-cholesterol (Austin et al., 1988; Bjornheden et al., 1996; Ivanova et al., 2017). In
800 future work, we want to evaluate whether the *mttp*$^{c655/c655}$ mutants are protected from
801 atherosclerosis because they produce fewer B-lps or are at higher risk because the B-lp
802 particles secreted are small and dense.
803
804 In conclusion, the unexpected discovery of the c655 missense mutation in *mttp* has provided
805 novel insight into the structure-function relationship of MTP, underlining the importance of
806 forward-genetic screening approaches to reveal aspects of biology that may otherwise be
807 missed. Our work provides the first evidence that the triglyceride and phospholipid transfer
808 functions of vertebrate MTP can be separated and that selective retention of phospholipid
809 transfer is sufficient for dietary fat absorption and normal growth. These results argue that
810 selective pharmacologic inhibition of triglyceride transfer may be a feasible therapeutic
811 approach to treat disorders of lipid metabolism.
812
813 **Acknowledgments**
814 We gratefully acknowledge Michael Sepanski for electron microscopy, Andrew Rock and
815 Carmen Tull for fish husbandry, Matthew Bray for assistance using R, Amy Kowalski for
816 synthesis of the pDESTTol2pA2-CMV: eGFP-CAAX plasmid, and Jennifer Anderson for help
817 editing the manuscript. We would also like to especially thank Philip Ingham, who provided the
818 *kif7* mutant strain in which we identified the *c655* mutation.
819
820 **Declaration of Interests**
821 Authors declare no competing interests.
822
823 **Supplementary Files**
824
825 Supplementary File 1: Single nucleotide variants present in *c655* mutant embryos.
826
827
828
829 **METHODS & MATERIALS**
830
831 ***Zebrafish husbandry and maintenance***
832 Adult zebrafish were maintained at 27°C on a 14:10h light:dark cycle and fed once daily with
833 ~3.5% body weight Gemma Micro 500 (Skretting USA). Embryos were obtained by natural
834 spawning and were raised in embryo medium at 28.5°C and kept on a 14:10 h light:dark cycle.

835 All embryos used for experiments were obtained from pair-wise crosses and were staged
836 according to (Kimmel et al., 1995). Exogenous food was provided starting at 5.5 days post
837 fertilization (dpf) unless otherwise noted. Larvae were fed with GEMMA Micro 75 (Skretting) 3x
838 a day until 14 dpf, GEMMA Micro 150 3x a day + Artemia 1x daily from 15 dpf–42 dpf and then
839 GEMMA Micro 500 daily supplemented once a week with Artemia. Zebrafish sex is not
840 determined until the juvenile stage, so gender is not a variable in experiments with embryos and
841 larvae. Sex of adult fish included in analyses is noted in Figure legends. All zebrafish protocols
842 were approved by the Carnegie Institution Department of Embryology Animal Care and Use
843 Committee (Protocol #139).
844
845 *Stalactite* (*stl*) *mttp* mutant zebrafish in the *Tg(fli1:eGFP)*^{y1} background (Avraham-Davidi et al.,
846 2012; Lawson and Weinstein, 2002; Yaniv et al., 2006) were provided by Karina Yaniv
847 (Weizmann Institute of Science, Israel) and out-crossed to the AB wild-type strain. The *stl*
848 mutation was maintained in both the presence and absence of the *fli1:eGFP* transgene. The
849 *c655* phenotype was identified in the Farber laboratory in the background of a *kif7* mutant strain
850 that was obtained from Philip Ingham (Lee Kong Chian School of Medicine, Singapore). The
851 *c655 mttp* mutation was isolated from the *kif7* mutation by out-crossing to the AB wild-type
852 strain. The *c655* mutation was crossed into the *Tg(fli1:eGFP)*^{Y1} reporter line. Both *stl* and *c655*
853 *mttp* mutations were crossed into the *ApoBb.1-NanoLuc* LipoGlo reporter line (Thierer et al., In
854 Press).
855
856
857 ***Positional Cloning***
858 To map the location of the mutation responsible for the c655 phenotype, 23 embryos with
859 normal yolks and 23 embryos with opaque yolks (3 dpf) were processed for RNA-seq (White et
860 al., 2017). RNA was extracted from embryos by mechanical lysis in RLT buffer (Qiagen, 79216)
861 containing 1 µL of 14.3M beta-mercaptoethanol (Sigma, M6250). The lysate was combined with
862 1.8 volumes of Agencourt RNAClean XP (Beckman Coulter, A63987) beads and allowed to bind
863 for 10 minutes. The plate was applied to a plate magnet (Invitrogen) until the solution cleared
864 and the supernatant was removed without disturbing the beads. This was followed by washing
865 the beads three times with 70% ethanol. After the last wash, the pellet was allowed to air dry for
866 10 mins and then resuspended in 50 µl of RNAse-free water. RNA was eluted from the beads
867 by applying the plate to the magnetic rack. RNA was quantified using the Quant-iT 610 RNA

868 assay (Invitrogen, Q33140). Total RNA from individual embryos was DNase treated for 20 mins
869 at 37°C followed by addition of 1 μL 0.5M EDTA and inactivation at 75°C for 10 mins to remove
870 residual DNA. RNA was then cleaned using 2 volumes of Agencourt RNAClean XP (Beckman
871 Coulter, A63987) beads under the standard protocol. Strand-specific RNA-seq libraries
872 containing unique index sequences in the adapter were generated simultaneously following the
873 dUTP method using 700 ng total RNA and ERCC spike mix 2 (Ambion, 4456740). Libraries
874 were pooled and sequenced on Illumina HiSeq 2500 in 75bp paired-end mode. Sequence data
875 were deposited in European Nucleotide Archive under accession ERP023267. FASTQ files
876 were aligned to the GRCz10 reference genome using TopHat2 (Kim et al., 2013) (v2.0.13,
877 options: --library-type fr-firststrand). Ensembl 88 gene models were supplied to TopHat2 to aid
878 transcriptome mapping. MMAPPR (Hill et al., 2013) was used to determine the location of the
879 causal mutation. Variants were called from the pooled data using the GATK HaplotypeCaller
880 (Van der Auwera et al., 2013). Variants inside the regions output by MMAPPR were selected
881 and filtered for ones where the mutant sample was called as being homozygous alternate and
882 the siblings were heterozygous. The consequences of these variants on annotated genes was
883 calculated using the Ensembl Variant Effect Predictor (McLaren et al., 2016) and SIFT (Sim et
884 al., 2012). Variants with the following consequences were selected as candidates for the causal
885 mutation: stop_gained, splice_donor_variant, splice_acceptor_variant, transcript_ablation,
886 frameshift_variant, stop_lost, initiator_codon_variant, missense_variant, inframe_insertion,
887 inframe_deletion, transcript_amplification, splice_region_variant,
888 incomplete_terminal_codon_variant.
889
890 ***DNA Extraction and Genotyping***
891 Genomic DNA was extracted from embryos or adult fin clips using a modified version of the
892 HotSHOT DNA extraction protocol (Meeker et al., 2007). Embryos/tissues were heated to 95°C
893 for 18 minutes in 100 μL of 50 mM NaOH. The solution was cooled to 25°C and neutralized
894 with 10 μL of 1M Tris-HCl pH 8.0. Genotyping primers for the stalactite allele were designed
895 using the dCAPS Finder 2.0 program (Neff et al., 2002) and synthesized by Eurofins Genomics.
896 The *stalactite* locus was amplified using the forward primer 5'-GTC TGA GGT TCA GAT GTA
897 CCT GTT AGG AC-3' and reverse primer 5'-CTC TGC TGT GAT GAG CGC AGG-3' (0.5 μM
898 primer, T_a = 60°C, extension time 30"). The forward primer introduces an AvaII restriction site
899 into the mutant amplicon, such that following digestion (5 units of AvaII (New England BioLabs,

900 R0153) at 37°C, 4 h) the WT band is 157bp, homozygous mutants have bands at 129 bp and 28
901 bp, and heterozygotes have all three bands. The *c655* locus was amplified using the forward
902 primer 5'-AGAGACGGTGTCCAAGCAGG-3' and reverse primer 5'-GCTCAAAGACTTTCTTGC-
903 3' (0.25 μM primer, Ta = 50°C, extension time 30"). The *c655* mutation introduces a BsrI
904 restriction site into the amplicon, such that following digestion (3 units of BsrI (New England
905 BioLabs, R0527) in NEB Buffer 3.1 (B7203), 65°C, 3.5 h) the WT band is 137 bp, homozygous
906 mutants have bands at 76 bp and 61 bp, and heterozygotes have all three bands. For the
907 *ApoBb.1-NanoLuc* genotyping protocol, see (Thierer et al., In Press).
908
909 ***Generation of mttp-FLAG and ApoB48 plasmids***
910 The wild-type zebrafish *mttp* coding sequence with a FLAG-tag prior to the termination codon at
911 the C-terminus was generated by custom gene synthesis and cloned into the pcDNA3.1+ vector
912 (*mttp*-FLAG)(Gene Universal Inc., Newark, DE). The *stl* and *c655* mutations were subsequently
913 introduced to this plasmid by site-directed mutagenesis (Gene Universal Inc.) to generate
914 $mttp^{stl}$-FLAG and $mttp^{c655}$-FLAG plasmids. The human pcDNA3.1-*MTTP*-FLAG plasmid was
915 synthesized as described previously (Rava et al., 2006; Sellers et al., 2003). The human
916 equivalent of the *c655* mutation (G865V) was introduced into this plasmid using the Q5 Site-
917 directed mutagenesis kit (New England Biolabs), with the following primer pair: Forward 5'-
918 CGTATTAGCAgtaTGTGAATTCC-3', Reverse 5- CTTTCTTTTCTTTTCTGAGAG-3'. The
919 human ApoB48 sequence (Hussain et al., 1995) was cloned into the pcDNA3 under control of
920 the CMV promoter.
921
922 ***Rescue of c655 opaque yolk phenotype***
923 $mttp^{c655/c655}$ embryos were injected at the 1-cell stage with 20pg of zebrafish *mttp*-FLAG plasmid
924 and 20 pg of CMV:*eGFP-CAAX* (synthesized using the Tol2kit Gateway cloning system using
925 the p5E-CMV/SP6, pME-*eGFP-CAAX*, and p3E-polyA entry clones (Kwan et al., 2007)) as a
926 marker of successful injections. Embryos were raised to 3 dpf and screened for eGFP
927 expression in the yolk sac. Images of eGFP+ control and experimental embryos were blinded
928 and scored for yolk opacity by another member of the lab.
929
930 ***Ectopic sprout analysis***
931 $mttp^{stl/stl}$, $mttp^{c655/c655}$ and WT zebrafish in the $Tg(fli1:eGFP)^{y1}$ background were imaged at 3 dpf
932 with a Zeiss Axiozoom V16 microscope equipped with a Zeiss PlanNeoFluar Z 1x/0.25 FWD

933 56mm objective, AxioCam MRm camera, and Zen 2.5 software. The length of ectopic
934 angiogenic segments that extend from the subintestinal vessels were analyzed in Fiji
935 (Schindelin et al., 2012)(ImageJ V2.0.0, National Institutes of Health, USA) as described by
936 (Avraham-Davidi et al., 2012).
937
938 ***Transmission Electron Microscopy***
939 Wild-type, *mttp*$^{stl/stl}$, *mttp*$^{c655/c655}$, and *mttp*$^{stl/c655}$ mutant zebrafish embryos were fixed at 4 dpf in a
940 3% glutaraldehyde, 1% formaldehyde, 0.1 M cacodylate solution for 1-3 h. Embryos were
941 trimmed and swim bladders were deflated before embedding in 2% low melt agarose and
942 processed as described in (Zeituni et al., 2016). Post-fixation was performed for 1 h with 1%
943 osmium tetroxide + 1.25% potassium ferricyanide in cacodylate solution. Following 2 x 10 min
944 washes with water, samples were incubated with 0.05M maleate pH 6.5 for 10 min. Samples
945 were stained en bloc with 0.5% uranyl acetate in maleate for 4°C overnight. Following 2 x 15
946 min washes with water, samples were dehydrated through graded EtOH dilution (35%, 2 x 15
947 min; 50%, 15 min; 75%, 15 min; 95%, 15 min; 100% 4 x 15 min). Samples were washed with
948 propylene oxide 4 x 15 min before incubation with 1:1 propylene oxide/resin (Epon 812 epoxy,
949 Ladd Research Industries, Williston, VT) for 1 h and evaporated overnight. This was followed
950 by 2 x 1 h washes in 100% resin and a final embedding in 100% resin at 55°C overnight
951 followed by 70°C for three days. Sections were made on a Reichert Ultracut-S (Leica
952 Microsystems), mounted on naked 200 thin mesh grids, and stained with lead citrate. Images
953 were obtained with a Phillips Technai-12 electron microscope (FEI, Hillsboro, OR) and 794
954 Gatan multiscan CCD camera (Gatan, Pleasanton, CA) using Digital Micrograph software. Lipid
955 droplet number and area was quantified with Fiji.
956
957 ***Growth Time-Course***
958 Unsorted embryos from pair-wise in-crosses of *stalactite* or *c655* heterozygous fish and pair-
959 wise crosses of *mttp*$^{stl/+}$ x *mttp*$^{c655/+}$ were raised and were analyzed for standard length at 1, 3, 6,
960 9, 12, and 24 weeks post fertilization. At 1 week, fish were imaged using a Nikon SMZ1500
961 microscope with HR Plan Apo 1x WD 54 objective, Infinity 3 Lumenera camera and Infinity
962 Analyze 6.5 software. Standard length (Parichy et al., 2009) was measured using Fiji (NIH).
963 Starting at three weeks, standard length was measured with a ruler. Mass of the fish was also
964 measured starting at 6 weeks. At 1 and 3 weeks, gDNA was obtained from whole fish for

965 genotyping. At later time-points, genotyping was performed on fin clips. Images of fish at 12
966 weeks post fertilization were taken with a Canon T6 camera with a Canon EF 100mm Macro
967 Lens.
968
969 ***Tissue Histology***
970 Adult zebrafish (7.5 mo; 2 males, 1 female per genotype) were placed individually into mating
971 tanks and fasted overnight (~24 h). Fish were euthanized by submersion in ice-water. A piece
972 of the anterior intestine and the liver were dissected from each animal and fixed in neutral-
973 buffered formalin (Sigma, F8775) at 4°C for 48 h. Sectioning and hematoxylin & eosin staining
974 was performed by the Johns Hopkins University Oncology Tissue Services. Slides were imaged
975 with a Nikon E800 microscope with 60×/1.4 oil Plan Apo Nikon objective and Canon EOS T3
976 camera using EOS Utility image acquisition software.
977
978 ***Tissue Lipid Extractions, HPLC & Analysis***
979 Adult zebrafish (1 yr; 2–3 males, 2–3 females per genotype) were fasted overnight (~24 h) and
980 euthanized by submersion in ice-water. Similar size pieces of the anterior intestine and the liver
981 were dissected from each animal and frozen on dry ice. Tissues were sonicated in 550 μL of
982 homogenization buffer (20 mM Tris-HCl, 1 mM EDTA), and the protein concentration of each
983 sample was measured using the BCA protein assay kit (Pierce, 23225). Lipids were extracted
984 from the remaining sample volume by a modified Bligh-Dyer procedure (Carten et al., 2011),
985 dried under vacuum, and re-suspended in 50 μL of HPLC-grade isopropanol as the HPLC
986 injection solvent. Injection volumes were optimized for each sample to produce peak shapes
987 appropriate for quantitation (1–25 μL). The lipid components of each sample were separated
988 and detected by an HPLC-CAD system using a LPG-3400RS quaternary pump, WPS-3000TRS
989 autosampler (maintained at 20°C), TCC-3000RS column oven (maintained at 40°C), Accucore
990 C18 column (150 x 3.0 mm, 2.6 μm particle size), FLD-3100 fluorescence detector (8 mL flow
991 cell maintained at 45°C), and a Dionex Corona Veo charged aerosol detector (Thermo Fisher
992 Scientific). Lipids were separated over an 80 min time range in a multi-step mobile phase
993 gradient as described in (Quinlivan et al., 2017). The lipid class and area of each analyte peak
994 were determined using Chromeleon 7.2 (Thermo-Fisher Scientific) for chromatogram
995 visualization and manual integration as described in (Otis et al., 2017). For quantitative

996 comparisons between samples, each lipid peak area was normalized to the protein
997 concentration of the homogenized tissue.
998
999 ***LipoGlo Assays***
1000 All LipoGlo assays were performed with fish carrying a single copy of the LipoGlo
1001 *(apoBb.1$^{NLuc/+}$)* reporter. For detailed LipoGlo methods see (Thierer et al., In Press); Nano-Glo
1002 reporter system reagents are all from Promega Corp., (N1110; (Hall et al., 2012)). For
1003 quantitative assays and B-lp size analysis, individual embryos were dispensed into 96-well
1004 plates (USAScientific, #1402-9589) and homogenized in 100 μL of B-lp stabilization buffer (40
1005 mM EGTA, pH 8.0, 20% sucrose + cOmplete mini, EDTA-free protease inhibitor (Sigma,
1006 11836170001)) by sonication in a microplate-horn sonicator (Qsonica Q700 sonicator with a
1007 Misonix CL-334 microplate horn assembly). Homogenate was stored on ice for immediate use
1008 or frozen at -20°C for later use. ApoB-Nanoluc levels were quantified by mixing 40 μL of
1009 embryo homogenate with an equal volume of diluted Nanoluc buffer (1:3 NanoGlo buffer:PBS +
1010 0.5% NanoLuc substrate (furimazine)) in a 96-well opaque white OptiPlate (Perkin-Elmer,
1011 6005290), and the plate was read within 2 minutes of buffer addition using a SpectraMax M5
1012 plate reader (Molecular Devices) set to top-read chemiluminescent detection with a 500 ms
1013 integration time. To quantify the size distribution of B-lps, 12 μL of homogenate was combined
1014 with 3 mL of 5x loading dye (40% sucrose, 0.25% bromophenol blue, in Tris/Borate/EDTA (TBE)
1015 buffer), and 12.5 mL of the resulting solution (10% larval homogenate) was loaded per well on a
1016 3% native polyacrylamide gel. Each gel included a migration standard of Di-I-labeled human
1017 LDL (L3482, ThermoFisher Scientific). Gels were run at 50V for 30 min, followed by 125V for 2
1018 h. Following application of 1 mL of TBE supplemented with 2 μL of Nano-Glo substrate to the
1019 surface of the gel and incubating for 5 min, gels were imaged with an Odyssey Fc (LI-COR
1020 Biosciences) gel imaging system. Images were obtained in the chemiluminescent channel (2
1021 min exposure) and then the 600 nm channel (30 sec) for Nanoluc detection and Di-I LDL
1022 standard detection, respectively. Each lane on the gel was converted to a plot profile in Fiji and
1023 divided into LDL, IDL, VLDL and Zero Mobility bins based on migration relative to the Di-I LDL
1024 standard. Pixel intensity from the plot profile was summed within each bin for comparison
1025 between genotypes. To determine the localization of B-lps in the whole fish, intact embryos or
1026 larvae were anesthetized and fixed in 4% paraformaldehyde for 3 h at room temperature.
1027 Following rinses in PBS + 0.1% tween-20 (3 x 15 min), embryos were mounted in 1% low-melt

1028 agarose (BP160-100, Fisher Scientific) in TBE supplemented with 1% Nano-Glo substrate.
1029 Chemiluminescent images (10 and 30 sec exposures with no illumination) and a brightfield
1030 image were taken with a Zeiss Axiozoom V16 microscope equipped with a Zeiss Plan NeoFluar
1031 Z 1x/0.25 FWD 56mm objective, AxioCam MRm camera, and Zen 2.5 software, using 2x2
1032 binning and 2x gain. Images were quantified using Fiji; regions of interest (ROI) were drawn on
1033 the brightfield image (viscera, trunk, and head), and these ROIs were used to quantify the
1034 NanoLuc intensity on the 30sec exposure chemiluminescent images. ROIs of the same shape
1035 were used to calculate the background signal, which was subtracted from the intensity value for
1036 each ROI.
1037
1038 ***Oil Red O staining***
1039 15-dpf larval zebrafish were fixed with 4% paraformaldehyde in PBS for 3 h at room
1040 temperature and then overnight at 4°C. Fish were rinsed in 60% 2-propanol for 10 minutes,
1041 rocking and then put into 0.3% Oil Red O (Sigma-Aldrich, #O0625) to rock overnight at room
1042 temperature. Fish were rinsed 3 times with 60% 2-propanol for 15 minutes. Washed fish were
1043 equilibrated step-wise into glycerol and imaged with incident light using a Nikon SMZ1500
1044 microscope with HR Plan Apo 1x WD 54 objective, Infinity 3 Lumenera camera, and Infinity
1045 Analyze 6.5 software.
1046
1047 ***ApoB secretion assays***
1048 Monkey kidney COS-7 cells which do not express MTTP or ApoB were plated in 10 cm^2 cell
1049 culture dishes at a density of 9 x 10^5 cells per plate and grown in Dulbecco's modified Eagle's
1050 medium (DMEM) containing 10% fetal bovine serum, L-glutamine, and antibiotics at 37°C.
1051 COS-7 cells were transfected with 5 µg of plasmid expressing human ApoB48 cDNA under the
1052 control of CMV promoter using endofectin (Genecopoeia, EF014) according to the
1053 manufacturer's protocol. After 24 hours, cells from each dish were harvested, equally distributed
1054 in 6-well plates, and reverse transfected with 3µg of either pcDNA3, pcDNA3-*mttp*-FLAG,
1055 pcDNA3-$mttp^{stl}$-FLAG, pcDNA3-$mttp^{c655}$-FLAG, pcDNA3-*MTTP*-FLAG, or pcDNA3-
1056 *MTTP*(G865V)-FLAG plasmids. After 32 h cells were incubated overnight with 1 mL of DMEM
1057 containing 10%FBS. The overnight conditioned media were collected to measure ApoB by
1058 ELISA (Bakillah et al., 1997; Hussain et al., 1995). Cells were scraped in PBS and a small
1059 aliquot was used to measure total protein using a Coomassie protein assay (Thermo Scientific,

1060 #1856209). Cells were lysed in cell extract buffer (100 mM Tris, pH 7.4, 150 mM NaCl, 1 mM
1061 EGTA, 1mM EDTA, 1% Triton X-100, 0.5% sodium deoxycholate). Lysates were rotated for 1 h
1062 at 4 ºC to solubilize the membranes and centrifuged at 16,000g for 30 mins. ApoB was
1063 measured in the supernatant via ELISA. Briefly, high binding 96 well plates (Corning, #3366)
1064 were incubated with capture antibody anti-LDL (apoB), clone 1D1(MyBiosource, #MBS465020,
1065 1:1000 dilution) overnight at room temperature. The plate was washed 3x with PBS-T (PBS +
1066 0.05% Tween-20) and blocked with 3% BSA (Boston Bio Products, #P753) for 1 h and washed
1067 3x with PBS-T, before incubating with 100 μL of standards and experimental samples for 3 h.
1068 The plate was washed 3x with PBST and incubated with 100 μL of human ApoB antibody
1069 (Academy Bio-Medical Company, Inc., #20S-G2, 1:1000 dilution) for 1 h. After washing the
1070 plate 3x with PBS-T, 100 μL of alkaline phosphatase labeled anti-goat IgG (Southern Biotech,
1071 #6300-04, 1:3000 dilution) was added to each well and incubated for 1 h. The plate was
1072 washed 3x with Diethanolamine buffer, pH 9.5 and 100 μl of PNPP (Thermo Scientific, #34045,
1073 1 mg/mL) was added to each well before reading the plate at 405nm in a PerkinElmer Victor^3
1074 1420 multilabel counter. Data for zebrafish and human plasmids were obtained in the same
1075 experiments, but are graphed separately in figures 5A,B & 6B,C; the pcDNA control data is
1076 displayed in both sets of graphs.
1077
1078 ***Immunofluorescence***
1079 COS-7 cells were plated at a density of 50,000 cells on coverslips in 12-well dishes and
1080 transfected with 2 μg of plasmids expressing either zebrafish or human MTTP-FLAG plasmids.
1081 After 48 h, cells were fixed in paraformaldehyde and blocked with PBS supplemented with 1 mM
1082 $MgCl_2$, 0.5 mM $CaCl_2$, 3% BSA, 0.1% Triton X-100 and 1% horse serum. Cells were incubated
1083 with anti-FLAG M2 monoclonal antibody (Sigma # F3165, 1:250 dilution) and anti-calnexin
1084 antibody (Santa Cruz Biotechnology, # sc-11397, 1:250 dilution) overnight. Cells were washed
1085 three times with PBS and incubated with goat anti-mouse Alexa Fluor-594 (Invitrogen, #A11005,
1086 1:500 dilution) and donkey anti-rabbit Alexa-Fluor-488 (Invitrogen, # A21206, 1:500 dilution) for
1087 1 h. The cells were washed and mounted with Vectashield mounting medium (Vector
1088 Laboratories, #H-1000). Images were taken on a Leica SP5II confocal microscope with a
1089 63x1.4 HCX PL Apo oil immersion lens.
1090
1091

1092 ***Immunoprecipitation and Western blotting***

1093 Transfected COS-7 cells were washed three times with ice cold PBS and scraped in buffer K (1
1094 mM Tris-HCl, 1 mM EGTA and 1 mM $MgCl_2$, pH 7.6) containing protease inhibitor cocktail
1095 (Sigma, # P2714). Cells were mechanically lysed by passing them 10 times with $30_{1/2}$-gauge
1096 needle and small fractions were used to measure the total protein using a Coomassie protein
1097 assay (Thermo Fisher Scientific, #1856209). Cell lysate was incubated with Anti-FLAG M2
1098 antibody for 1 h and immunoprecipitated (IP) using (protein A/G) agarose beads (Santa-Cruz
1099 Biotechnology, # SC2003). The supernatants were used to detect actin via Western blotting
1100 and served as loading controls. Both the supernatant and immunoprecipitated fractions were
1101 subjected to electrophoresis on an 8% SDS-PAGE gel. The weight separated proteins were
1102 transferred to nitrocellulose membranes and probed with either anti-FLAG M2 (1:1000) or anti-
1103 actin (Thermo Fisher Scientific, #PA1-183, (1:3000)) prepared in 2% BSA in TBS. The blots
1104 were washed and probed with HRP-conjugated corresponding secondary antibodies (goat anti-
1105 rabbit, Cell Signaling Technology, #7074, 1:5000 or goat anti-mouse, Thermo Fisher Scientific,
1106 #62-6520, 1:5000). The blots were developed in ChemiDoc™-Touch Imaging system from Bio
1107 Rad.

1108

1109 ***Triglyceride transfer assay***

1110 Following transfection with plasmids as described above, cell lysate (35 µg) prepared in buffer K
1111 containing protease inhibitor cocktail was incubated with donor vesicles containing NBD-labeled
1112 triolein (Setareh Biotech, LLC, #6285) and acceptor vesicles. Fluorescence was measured at
1113 different time intervals (5, 10, 15, 30, 45 and 60 mins). Percent triglyceride transfer was
1114 calculated after subtracting the blank and dividing it by the total fluorescence reading obtained
1115 by disrupting vesicles with isopropanol, as described previously (Athar et al., 2004; Rava et al.,
1116 2005). Where noted, assays also included the MTTP inhibitor Lomitapide (Aegerion
1117 Pharmaceuticals, #AEGR-733) at a concentration of 1 µM.

1118

1119 ***Phospholipid transfer assay***

1120 COS-7 cells were transfected with 9 µg of either zebrafish *mttp*-FLAG or human MTTP-FLAG
1121 plasmids in 10 cm^2 cell culture dishes. After 48 h, cell lysates were prepared in buffer K
1122 containing protease inhibitor cocktail (Sigma, #P2714). The cell lysates were centrifuged at
1123 12,000g for 10 mins at 4ºC. A small aliquot of cell lysate was used for measuring protein and
1124 kept for Western blotting to measure expression level. Equal concentrations of protein from

1125 each sample were incubated with 40 µL of M2 agarose beads (Sigma, #A2220) for 3 h at 4ºC.
1126 FLAG-tagged protein were eluted twice with 200 ng/µL FLAG peptide (Sigma, #F3290; 1 h at
1127 4ºC). PL transfer activity was assayed using NBD labeled Phosphoethanolamine,
1128 triethylammonium (Thermo Fisher Scientific, #N360). The purified FLAG-tagged proteins were
1129 incubated with donor vesicles containing NBD-Phosphoethanolamine and acceptor vesicles.
1130 The fluorescence was measured at different time intervals (1, 2, 3 and 4 h). The percentage
1131 transfer of phospholipid was calculated as the difference between the fluorescence reading at
1132 the 0 h time point and 3 h time point divided by the total fluorescence reading obtained by
1133 disrupting vesicles with isopropanol as described previously (Athar et al., 2004; Rava et al.,
1134 2005). Where noted, assays also included the MTTP inhibitor Lomitapide at a concentration of
1135 1 µM.
1136
1137 ***Modeling***
1138 Predicted models of human MTTP and zebrafish Mttp proteins were generated using Phyre2
1139 (Kelley et al., 2015) and the graphics were enhanced for clarity using Chimera (UCSF Chimera,
1140 developed by the Resource for Biocomputing, Visualization, and Informatics at the University of
1141 California, San Francisco, with support from NIH P41-GM103311 (Pettersen et al., 2004).
1142
1143 ***Statistical Analyses***
1144 Graphing and some statistics, including One-way, randomized block and Repeated Measures
1145 ANOVA with Bonferroni post-hoc tests, Kruskall-Wallis with Dunn's Multiple Comparison test
1146 and Chi-square tests were performed with GraphPad Prism (GraphPad Software). When
1147 sample sizes and variance between groups were significantly different, Robust ANOVA was
1148 performed using R to determine overall significance of noted datasets (Mair and Wilcox,
1149 2018)(https://cran.r-project.org/web/packages/WRS2/vignettes/WRS2.pdf),((Mangiafico, 2015),
1150 https://rcompanion.org/rcompanion/d_08a.html). When significant differences were present
1151 between genotypes, Games-Howell post-hoc tests were used to make pair-wise comparisons at
1152 each time point using SPSS Statistics (IBM), adjusting the significance level for multiple
1153 comparisons. Details of the statistical analyses can be found either in the figure legend or
1154 results sections. Sample sizes for each experiment are indicated in the figure legends for each
1155 experiment.
1156
1157

1158 ***Additional Software***

1159 DNA, mRNA, and protein sequence alignments were performed with MacVector V15.5
1160 (MacVector, Inc.). Microsoft Word and Excel were used for manuscript preparation and data
1161 analysis, respectively, figures were assembled in Adobe Illustrator CS5 (Adobe Systems) and
1162 references were assembled with EndNote 8X.

1163
1164
1165
1166 **REFERENCES**
1167

1168 Alexander, C.A., Hamilton, R.L., and Havel, R.J. (1976). Subcellular localization of B apoprotein
1169 of plasma lipoproteins in rat liver. J Cell Biol *69*, 241-263.

1170 Anderson, T.A., Levitt, D.G., and Banaszak, L.J. (1998). The structural basis of lipid interactions
1171 in lipovitellin, a soluble lipoprotein. Structure *6*, 895-909.

1172 Athar, H., Iqbal, J., Jiang, X.C., and Hussain, M.M. (2004). A simple, rapid, and sensitive
1173 fluorescence assay for microsomal triglyceride transfer protein. J Lipid Res *45*, 764-772.

1174 Atzel, A., and Wetterau, J.R. (1993). Mechanism of microsomal triglyceride transfer protein
1175 catalyzed lipid transport. Biochemistry *32*, 10444-10450.

1176 Atzel, A., and Wetterau, J.R. (1994). Identification of two classes of lipid molecule binding sites
1177 on the microsomal triglyceride transfer protein. Biochemistry *33*, 15382-15388.

1178 Austin, M.A., Breslow, J.L., Hennekens, C.H., Buring, J.E., Willett, W.C., and Krauss, R.M.
1179 (1988). Low-density lipoprotein subclass patterns and risk of myocardial infarction. JAMA *260*,
1180 1917-1921.

1181 Avraham-Davidi, I., Ely, Y., Pham, V.N., Castranova, D., Grunspan, M., Malkinson, G., Gibbs-
1182 Bar, L., Mayseless, O., Allmog, G., Lo, B., et al. (2012). ApoB-containing lipoproteins regulate
1183 angiogenesis by modulating expression of VEGF receptor 1. Nat Med *18*, 967-973.

1184 Bakillah, A., Zhou, Z., Luchoomun, J., and Hussain, M.M. (1997). Measurement of
1185 apolipoprotein B in various cell lines: correlation between intracellular levels and rates of
1186 secretion. Lipids *32*, 1113-1118.

1187 Banaszak, L., Sharrock, W., and Timmins, P. (1991). Structure and function of a lipoprotein:
1188 lipovitellin. Annu Rev Biophys Biophys Chem *20*, 221-246.

1189 Berthier, M.T., Couture, P., Houde, A., Paradis, A.M., Sammak, A., Verner, A., Depres, J.P.,
1190 Gagne, C., Gaudet, D., and Vohl, M.C. (2004). The c.419-420insA in the MTP gene is
1191 associated with abetalipoproteinemia among French-Canadians. Mol Genet Metab *81*, 140-143.

1192 Bjornheden, T., Babyi, A., Bondjers, G., and Wiklund, O. (1996). Accumulation of lipoprotein
1193 fractions and subfractions in the arterial wall, determined in an in vitro perfusion system.
1194 Atherosclerosis *123*, 43-56.

1195 Blom, D.J., Averna, M.R., Meagher, E.A., du Toit Theron, H., Sirtori, C.R., Hegele, R.A., Shah,
1196 P.K., Gaudet, D., Stefanutti, C., Vigna, G.B., et al. (2017). Long-Term Efficacy and Safety of the
1197 Microsomal Triglyceride Transfer Protein Inhibitor Lomitapide in Patients With Homozygous
1198 Familial Hypercholesterolemia. Circulation *136*, 332-335.

1199 Boren, J., Rustaeus, S., and Olofsson, S.O. (1994). Studies on the assembly of apolipoprotein
1200 B-100- and B-48-containing very low density lipoproteins in McA-RH7777 cells. J Biol Chem
1201 *269*, 25879-25888.

1202 Bradbury, P., Mann, C.J., Kochl, S., Anderson, T.A., Chester, S.A., Hancock, J.M., Ritchie, P.J.,
1203 Amey, J., Harrison, G.B., Levitt, D.G., et al. (1999). A common binding site on the microsomal
1204 triglyceride transfer protein for apolipoprotein B and protein disulfide isomerase. J Biol Chem
1205 *274*, 3159-3164.

1206 Carten, J.D., Bradford, M.K., and Farber, S.A. (2011). Visualizing digestive organ morphology
1207 and function using differential fatty acid metabolism in live zebrafish. Dev Biol *360*, 276-285.

1208 Carvalho, L., and Heisenberg, C.P. (2010). The yolk syncytial layer in early zebrafish
1209 development. Trends Cell Biol *20*, 586-592.

1210 CDC (2018). Centers for Disease Control and Prevention, National Center for Health Statistics.
1211 Underlying Cause of Death 1999-2017 on CDC WONDER Online Database, released
1212 December, 2018. Data are from the Multiple Cause of Death Files, 1999-2017, as compiled
1213 from data provided by the 57 vital statistics jurisdictions through the Vital Statistics Cooperative
1214 Program. In http://wonder.cdc.gov/ucd-icd10.html (Centers for Disease Control).

1215 Cuchel, M., Bloedon, L.T., Szapary, P.O., Kolansky, D.M., Wolfe, M.L., Sarkis, A., Millar, J.S.,
1216 Ikewaki, K., Siegelman, E.S., Gregg, R.E., et al. (2007). Inhibition of microsomal triglyceride
1217 transfer protein in familial hypercholesterolemia. N Engl J Med *356*, 148-156.

1218 Cuchel, M., Bruckert, E., Ginsberg, H.N., Raal, F.J., Santos, R.D., Hegele, R.A., Kuivenhoven,
1219 J.A., Nordestgaard, B.G., Descamps, O.S., Steinhagen-Thiessen, E., et al. (2014). Homozygous
1220 familial hypercholesterolaemia: new insights and guidance for clinicians to improve detection
1221 and clinical management. A position paper from the Consensus Panel on Familial
1222 Hypercholesterolaemia of the European Atherosclerosis Society. Eur Heart J *35*, 2146-2157.

1223 Cuchel, M., Meagher, E.A., du Toit Theron, H., Blom, D.J., Marais, A.D., Hegele, R.A., Averna,
1224 M.R., Sirtori, C.R., Shah, P.K., Gaudet, D., et al. (2013). Efficacy and safety of a microsomal
1225 triglyceride transfer protein inhibitor in patients with homozygous familial hypercholesterolaemia:
1226 a single-arm, open-label, phase 3 study. Lancet *381*, 40-46.

1227 Davidson, N.O., and Shelness, G.S. (2000). APOLIPOPROTEIN B: mRNA editing, lipoprotein
1228 assembly, and presecretory degradation. Annu Rev Nutr *20*, 169-193.

1229 Di Filippo, M., Collardeau Frachon, S., Janin, A., Rajan, S., Marmontel, O., Decourt, C., Rubio,
1230 A., Nony, S., Dumont, S., Cuerq, C., et al. (2019). Normal serum ApoB48 and red cells vitamin
1231 E concentrations after supplementation in a novel compound heterozygous case of
1232 abetalipoproteinemia. Atherosclerosis *284*, 75-82.

1233 Di Filippo, M., Crehalet, H., Samson-Bouma, M.E., Bonnet, V., Aggerbeck, L.P., Rabes, J.P.,
1234 Gottrand, F., Luc, G., Bozon, D., and Sassolas, A. (2012). Molecular and functional analysis of
1235 two new MTTP gene mutations in an atypical case of abetalipoproteinemia. J Lipid Res *53*, 548-
1236 555.

1237 Di Leo, E., Lancellotti, S., Penacchioni, J.Y., Cefalu, A.B., Averna, M., Pisciotta, L., Bertolini, S.,
1238 Calandra, S., Gabelli, C., and Tarugi, P. (2005). Mutations in MTP gene in abeta- and hypobeta-
1239 lipoproteinemia. Atherosclerosis *180*, 311-318.

1240 Dougan, S.K., Salas, A., Rava, P., Agyemang, A., Kaser, A., Morrison, J., Khurana, A.,
1241 Kronenberg, M., Johnson, C., Exley, M., et al. (2005). Microsomal triglyceride transfer protein
1242 lipidation and control of CD1d on antigen-presenting cells. J Exp Med *202*, 529-539.

1243 Elovson, J., Chatterton, J.E., Bell, G.T., Schumaker, V.N., Reuben, M.A., Puppione, D.L.,
1244 Reeve, J.R., Jr., and Young, N.L. (1988). Plasma very low density lipoproteins contain a single
1245 molecule of apolipoprotein B. J Lipid Res *29*, 1461-1473.

1246 Farese, R.V., Jr., Cases, S., Ruland, S.L., Kayden, H.J., Wong, J.S., Young, S.G., and
1247 Hamilton, R.L. (1996). A novel function for apolipoprotein B: lipoprotein synthesis in the yolk sac
1248 is critical for maternal-fetal lipid transport in mice. J Lipid Res *37*, 347-360.

1249 FDA (2012). JUXTAPID TM (lomitapide) capsules, for oral use Initial U.S. Approval: 2012 In
1250 https://www.accessdata.fda.gov/drugsatfda_docs/label/2012/203858s000lbl.Pdf.

1251 Fraher, D., Sanigorski, A., Mellett, N.A., Meikle, P.J., Sinclair, A.J., and Gibert, Y. (2016).
1252 Zebrafish Embryonic Lipidomic Analysis Reveals that the Yolk Cell Is Metabolically Active in
1253 Processing Lipid. Cell Rep *14*, 1317-1329.

1254 Glickman, R.M., Khorana, J., and Kilgore, A. (1976). Localization of apolipoprotein B in intestinal
1255 epithelial cells. Science *193*, 1254-1255.

1256 Hall, M.P., Unch, J., Binkowski, B.F., Valley, M.P., Butler, B.L., Wood, M.G., Otto, P.,
1257 Zimmerman, K., Vidugiris, G., Machleidt, T., et al. (2012). Engineered luciferase reporter from a
1258 deep sea shrimp utilizing a novel imidazopyrazinone substrate. ACS Chem Biol *7*, 1848-1857.

1259 Hamilton, R.L., Wong, J.S., Cham, C.M., Nielsen, L.B., and Young, S.G. (1998). Chylomicron-
1260 sized lipid particles are formed in the setting of apolipoprotein B deficiency. J Lipid Res *39*,
1261 1543-1557.

1262 Hill, J.T., Demarest, B.L., Bisgrove, B.W., Gorsi, B., Su, Y.C., and Yost, H.J. (2013). MMAPPR:
1263 mutation mapping analysis pipeline for pooled RNA-seq. Genome Res *23*, 687-697.

1264 Hiramatsu, N., Todo, T., Sullivan, C.V., Schilling, J., Reading, B.J., Matsubara, T., Ryu, Y.W.,
1265 Mizuta, H., Luo, W., Nishimiya, O., et al. (2015). Ovarian yolk formation in fishes: Molecular
1266 mechanisms underlying formation of lipid droplets and vitellogenin-derived yolk proteins. Gen
1267 Comp Endocrinol *221*, 9-15.

1268 Hussain, M.M., and Bakillah, A. (2008). New approaches to target microsomal triglyceride
1269 transfer protein. Curr. Opin. Lipidol *19*, 572-578.

1270 Hussain, M.M., Iqbal, J., Anwar, K., Rava, P., and Dai, K. (2003a). Microsomal triglyceride
1271 transfer protein: a multifunctional protein. Front Biosci *8*, s500-506.

1272 Hussain, M.M., Kancha, R.K., Zhou, Z., Luchoomun, J., Zu, H., and Bakillah, A. (1996).
1273 Chylomicron assembly and catabolism: role of apolipoproteins and receptors. Biochim Biophys
1274 Acta *1300*, 151-170.

1275 Hussain, M.M., Shi, J., and Dreizen, P. (2003b). Microsomal triglyceride transfer protein and its
1276 role in apoB-lipoprotein assembly. J Lipid Res *44*, 22-32.

1277 Hussain, M.M., Zhao, Y., Kancha, R.K., Blackhart, B.D., and Yao, Z. (1995). Characterization of
1278 recombinant human apoB-48-containing lipoproteins in rat hepatoma McA-RH7777 cells
1279 transfected with apoB-48 cDNA. Overexpression of apoB-48 decreases synthesis of
1280 endogenous apoB-100. Arterioscler Thromb Vasc Biol *15*, 485-494.

1281 Hwang, H.S., Xie, Y., Koudouna, E., Na, K.S., Yoo, Y.S., Yang, S.W., Brown, D.J., and Jester,
1282 J.V. (2018). Light transmission/absorption characteristics of the meibomian gland. Ocul Surf *16*,
1283 448-453.

1284 Iqbal, J., Walsh, M.T., Hammad, S.M., Cuchel, M., Tarugi, P., Hegele, R.A., Davidson, N.O.,
1285 Rader, D.J., Klein, R.L., and Hussain, M.M. (2015). Microsomal Triglyceride Transfer Protein
1286 Transfers and Determines Plasma Concentrations of Ceramide and Sphingomyelin but Not
1287 Glycosylceramide. J Biol Chem *290*, 25863-25875.

1288 Ivanova, E.A., Myasoedova, V.A., Melnichenko, A.A., Grechko, A.V., and Orekhov, A.N. (2017).
1289 Small Dense Low-Density Lipoprotein as Biomarker for Atherosclerotic Diseases. Oxid Med Cell
1290 Longev *2017*, 1273042.

1291 Jamil, H., Dickson, J.K., Jr., Chu, C.H., Lago, M.W., Rinehart, J.K., Biller, S.A., Gregg, R.E., and
1292 Wetterau, J.R. (1995). Microsomal triglyceride transfer protein. Specificity of lipid binding and
1293 transport. J Biol Chem *270*, 6549-6554.

1294 Jamil, H., Gordon, D.A., Eustice, D.C., Brooks, C.M., Dickson, J.K., Jr., Chen, Y., Ricci, B., Chu,
1295 C.H., Harrity, T.W., Ciosek, C.P., Jr., et al. (1996). An inhibitor of the microsomal triglyceride
1296 transfer protein inhibits apoB secretion from HepG2 cells. Proc Natl Acad Sci U S A *93*, 11991-
1297 11995.

1298 Kane, J.P., Hardman, D.A., and Paulus, H.E. (1980). Heterogeneity of apolipoprotein B:
1299 isolation of a new species from human chylomicrons. Proc Natl Acad Sci U S A *77*, 2465-2469.

1300 Kane, J.P.H., R. J. (1995). Disorders of the biogenesis and secretion of lipoproteins containing
1301 the B apolipoproteins. In The metabolic and molecular bases of inherited disorders. A.L.B. C. R.
1302 Scriver, W. S. Sly and D. Valle., ed. (New York: McGraw-Hill, Inc.), pp. 1853-1885.

1303 Kelley, L.A., Mezulis, S., Yates, C.M., Wass, M.N., and Sternberg, M.J. (2015). The Phyre2 web
1304 portal for protein modeling, prediction and analysis. Nat Protoc *10*, 845-858.

1305 Kessler, J.I., Stein, J., Dannacker, D., and Narcessian, P. (1970). Biosynthesis of low density
1306 lipoprotein by cell-free preparations of rat intestinal mucosa. J Biol Chem *245*, 5281-5288.

1307 Khatun, I., Walsh, M.T., and Hussain, M.M. (2013). Loss of both phospholipid and triglyceride
1308 transfer activities of microsomal triglyceride transfer protein in abetalipoproteinemia. J Lipid Res
1309 *54*, 1541-1549.

1310 Khatun, I., Zeissig, S., Iqbal, J., Wang, M., Curiel, D., Shelness, G.S., Blumberg, R.S., and
1311 Hussain, M.M. (2012). Phospholipid transfer activity of microsomal triglyceride transfer protein
1312 produces apolipoprotein B and reduces hepatosteatosis while maintaining low plasma lipids in
1313 mice. Hepatology *55*, 1356-1368.

1314 Kim, D., Pertea, G., Trapnell, C., Pimentel, H., Kelley, R., and Salzberg, S.L. (2013). TopHat2:
1315 accurate alignment of transcriptomes in the presence of insertions, deletions and gene fusions.
1316 Genome Biol *14*, R36.

1317 Kimmel, C.B., Ballard, W.W., Kimmel, S.R., Ullmann, B., and Schilling, T.F. (1995). Stages of
1318 embryonic development of the zebrafish. Dev Dyn *203*, 253-310.

1319 Kimmel, C.B., and Law, R.D. (1985). Cell lineage of zebrafish blastomeres. II. Formation of the
1320 yolk syncytial layer. Dev Biol *108*, 86-93.

1321 Kulinski, A., Rustaeus, S., and Vance, J.E. (2002). Microsomal triacylglycerol transfer protein is
1322 required for lumenal accretion of triacylglycerol not associated with ApoB, as well as for ApoB
1323 lipidation. J Biol Chem *277*, 31516-31525.

1324 Kwan, K.M., Fujimoto, E., Grabher, C., Mangum, B.D., Hardy, M.E., Campbell, D.S., Parant,
1325 J.M., Yost, H.J., Kanki, J.P., and Chien, C.B. (2007). The Tol2kit: a multisite gateway-based
1326 construction kit for Tol2 transposon transgenesis constructs. Dev Dyn *236*, 3088-3099.

1327 Lawson, N.D., and Weinstein, B.M. (2002). In vivo imaging of embryonic vascular development
1328 using transgenic zebrafish. Dev Biol *248*, 307-318.

1329 Lee, J., and Hegele, R.A. (2014). Abetalipoproteinemia and homozygous
1330 hypobetalipoproteinemia: a framework for diagnosis and management. J Inherit Metab Dis *37*,
1331 333-339.

1332 Madsen, E.M., Lindegaard, M.L., Andersen, C.B., Damm, P., and Nielsen, L.B. (2004). Human
1333 placenta secretes apolipoprotein B-100-containing lipoproteins. J Biol Chem *279*, 55271-55276.

1334 Mahley, R.W., Bersot, T.P., LeQuire, V.S., Levy, R.I., Windmueller, H.G., and Brown, W.V.
1335 (1970). Identity of very low density lipoprotein apoproteins of plasma and liver Golgi apparatus.
1336 Science *168*, 380-382.

1337 Mair, P., and Wilcox, R. (2018). Robust Statistical Methods Using WRS2. In https://cran.r-
1338 project.org/web/packages/WRS2/vignettes/WRS2.pdf.

1339 Mangiafico, S.S. (2015). An R Companion for the Handbook of Biological Statistics, version
1340 1.3.2. In https://rcompanion.org/rcompanion/d_08a.html.

1341 Mani-Ponset, L., Guyot, E., Diaz, J., and Connes, R. (1996). Utilization of yolk reserves during
1342 post-embryonic development in three teleostean species: the sea bream Sparus aurata, the sea

1343 bass Dicentrarchus labrax, and the pike-perch Stizostedion lucioperca. Marine Biology *126*,
1344 539-547.

1345 Mann, C.J., Anderson, T.A., Read, J., Chester, S.A., Harrison, G.B., Kochl, S., Ritchie, P.J.,
1346 Bradbury, P., Hussain, F.S., Amey, J., et al. (1999). The structure of vitellogenin provides a
1347 molecular model for the assembly and secretion of atherogenic lipoproteins. J Mol Biol *285*,
1348 391-408.

1349 Marza, E., Barthe, C., Andre, M., Villeneuve, L., Helou, C., and Babin, P.J. (2005).
1350 Developmental expression and nutritional regulation of a zebrafish gene homologous to
1351 mammalian microsomal triglyceride transfer protein large subunit. Dev Dyn *232*, 506-518.

1352 McLaren, W., Gil, L., Hunt, S.E., Riat, H.S., Ritchie, G.R., Thormann, A., Flicek, P., and
1353 Cunningham, F. (2016). The Ensembl Variant Effect Predictor. Genome Biol *17*, 122.

1354 Meeker, N.D., Hutchinson, S.A., Ho, L., and Trede, N.S. (2007). Method for isolation of PCR-
1355 ready genomic DNA from zebrafish tissues. Biotechniques *43*, 610, 612, 614.

1356 Michels, R., Foschum, F., and Kienle, A. (2008). Optical properties of fat emulsions. Opt
1357 Express *16*, 5907-5925.

1358 Miller, S.A., Burnett, J.R., Leonis, M.A., McKnight, C.J., van Bockxmeer, F.M., and Hooper, A.J.
1359 (2014). Novel missense MTTP gene mutations causing abetalipoproteinemia. Biochim Biophys
1360 Acta *1842*, 1548-1554.

1361 Miyares, R.L., de Rezende, V.B., and Farber, S.A. (2014). Zebrafish yolk lipid processing: a
1362 tractable tool for the study of vertebrate lipid transport and metabolism. Dis Model Mech *7*, 915-
1363 927.

1364 Narcisi, T.M., Shoulders, C.C., Chester, S.A., Read, J., Brett, D.J., Harrison, G.B., Grantham,
1365 T.T., Fox, M.F., Povey, S., de Bruin, T.W., et al. (1995). Mutations of the microsomal
1366 triglyceride-transfer-protein gene in abetalipoproteinemia. Am J Hum Genet *57*, 1298-1310.

1367 Neff, M.M., Turk, E., and Kalishman, M. (2002). Web-based primer design for single nucleotide
1368 polymorphism analysis. Trends Genet *18*, 613-615.

1369 Olzmann, J.A., and Carvalho, P. (2019). Dynamics and functions of lipid droplets. Nat Rev Mol
1370 Cell Biol *20*, 137-155.

1371 Otis, J.P., and Farber, S.A. (2016). High-fat Feeding Paradigm for Larval Zebrafish: Feeding,
1372 Live Imaging, and Quantification of Food Intake. J Vis Exp.

1373 Otis, J.P., Shen, M.C., Quinlivan, V., Anderson, J.L., and Farber, S.A. (2017). Intestinal
1374 epithelial cell caveolin 1 regulates fatty acid and lipoprotein cholesterol plasma levels. Dis Model
1375 Mech *10*, 283-295.

1376 Otis, J.P., Zeituni, E.M., Thierer, J.H., Anderson, J.L., Brown, A.C., Boehm, E.D., Cerchione,
1377 D.M., Ceasrine, A.M., Avraham-Davidi, I., Tempelhof, H., et al. (2015). Zebrafish as a model for
1378 apolipoprotein biology: comprehensive expression analysis and a role for ApoA-IV in regulating
1379 food intake. Dis Model Mech *8*, 295-309.

1380 Parichy, D.M., Elizondo, M.R., Mills, M.G., Gordon, T.N., and Engeszer, R.E. (2009). Normal
1381 table of postembryonic zebrafish development: staging by externally visible anatomy of the
1382 living fish. Dev Dyn *238*, 2975-3015.

1383 Patel, S.B., and Grundy, S.M. (1996). Interactions between microsomal triglyceride transfer
1384 protein and apolipoprotein B within the endoplasmic reticulum in a heterologous expression
1385 system. J Biol Chem *271*, 18686-18694.

1386 Pettersen, E.F., Goddard, T.D., Huang, C.C., Couch, G.S., Greenblatt, D.M., Meng, E.C., and
1387 Ferrin, T.E. (2004). UCSF Chimera--a visualization system for exploratory research and
1388 analysis. J Comput Chem *25*, 1605-1612.

1389 Plonne, D., Winkler, L., Franke, H., and Dargel, R. (1992). The visceral yolk sac--an important
1390 site of synthesis and secretion of apolipoprotein B containing lipoproteins in the feto-placental
1391 unit of the rat. Biochim Biophys Acta *1127*, 174-185.

1392 Quinlivan, V.H., Wilson, M.H., Ruzicka, J., and Farber, S.A. (2017). An HPLC-CAD/fluorescence
1393 lipidomics platform using fluorescent fatty acids as metabolic tracers. J Lipid Res *58*, 1008-
1394 1020.

1395 Raabe, M., Flynn, L.M., Zlot, C.H., Wong, J.S., Veniant, M.M., Hamilton, R.L., and Young, S.G.
1396 (1998). Knockout of the abetalipoproteinemia gene in mice: reduced lipoprotein secretion in
1397 heterozygotes and embryonic lethality in homozygotes. Proc Natl Acad Sci U S A *95*, 8686-
1398 8691.

1399 Raabe, M., Veniant, M.M., Sullivan, M.A., Zlot, C.H., Bjorkegren, J., Nielsen, L.B., Wong, J.S.,
1400 Hamilton, R.L., and Young, S.G. (1999). Analysis of the role of microsomal triglyceride transfer
1401 protein in the liver of tissue-specific knockout mice. J Clin Invest *103*, 1287-1298.

1402 Raag, R., Appelt, K., Xuong, N.H., and Banaszak, L. (1988). Structure of the lamprey yolk lipid-
1403 protein complex lipovitellin-phosvitin at 2.8 A resolution. J Mol Biol *200*, 553-569.

1404 Rava, P., Athar, H., Johnson, C., and Hussain, M.M. (2005). Transfer of cholesteryl esters and
1405 phospholipids as well as net deposition by microsomal triglyceride transfer protein. J Lipid Res
1406 *46*, 1779-1785.

1407 Rava, P., and Hussain, M.M. (2007). Acquisition of triacylglycerol transfer activity by microsomal
1408 triglyceride transfer protein during evolution. Biochemistry *46*, 12263-12274.

1409 Rava, P., Ojakian, G.K., Shelness, G.S., and Hussain, M.M. (2006). Phospholipid transfer
1410 activity of microsomal triacylglycerol transfer protein is sufficient for the assembly and secretion
1411 of apolipoprotein B lipoproteins. J Biol Chem *281*, 11019-11027.

1412 Read, J., Anderson, T.A., Ritchie, P.J., Vanloo, B., Amey, J., Levitt, D., Rosseneu, M., Scott, J.,
1413 and Shoulders, C.C. (2000). A mechanism of membrane neutral lipid acquisition by the
1414 microsomal triglyceride transfer protein. J Biol Chem *275*, 30372-30377.

1415 Rehberg, E.F., Samson-Bouma, M.E., Kienzle, B., Blinderman, L., Jamil, H., Wetterau, J.R.,
1416 Aggerbeck, L.P., and Gordon, D.A. (1996). A novel abetalipoproteinemia genotype.
1417 Identification of a missense mutation in the 97-kDa subunit of the microsomal triglyceride

1418 transfer protein that prevents complex formation with protein disulfide isomerase. J Biol Chem
1419 *271*, 29945-29952.

1420 Ricci, B., Sharp, D., O'Rourke, E., Kienzle, B., Blinderman, L., Gordon, D., Smith-Monroy, C.,
1421 Robinson, G., Gregg, R.E., Rader, D.J., et al. (1995). A 30-amino acid truncation of the
1422 microsomal triglyceride transfer protein large subunit disrupts its interaction with protein
1423 disulfide-isomerase and causes abetalipoproteinemia. J Biol Chem *270*, 14281-14285.

1424 Robl, J.A., Sulsky, R., Sun, C.Q., Simpkins, L.M., Wang, T., Dickson, J.K., Jr., Chen, Y.,
1425 Magnin, D.R., Taunk, P., Slusarchyk, W.A., et al. (2001). A novel series of highly potent
1426 benzimidazole-based microsomal triglyceride transfer protein inhibitors. J Med Chem *44*, 851-
1427 856.

1428 Schindelin, J., Arganda-Carreras, I., Frise, E., Kaynig, V., Longair, M., Pietzsch, T., Preibisch,
1429 S., Rueden, C., Saalfeld, S., Schmid, B., et al. (2012). Fiji: an open-source platform for
1430 biological-image analysis. Nat Methods *9*, 676-682.

1431 Schlegel, A., and Stainier, D.Y. (2006). Microsomal triglyceride transfer protein is required for
1432 yolk lipid utilization and absorption of dietary lipids in zebrafish larvae. Biochemistry *45*, 15179-
1433 15187.

1434 Schumaker, V.N., Phillips, M.L., and Chatterton, J.E. (1994). Apolipoprotein B and low-density
1435 lipoprotein structure: implications for biosynthesis of triglyceride-rich lipoproteins. Adv Protein
1436 Chem *45*, 205-248.

1437 Sellers, J.A., Hou, L., Athar, H., Hussain, M.M., and Shelness, G.S. (2003). A Drosophila
1438 microsomal triglyceride transfer protein homolog promotes the assembly and secretion of
1439 human apolipoprotein B. Implications for human and insect transport and metabolism. J Biol
1440 Chem *278*, 20367-20373.

1441 Sharp, D., Blinderman, L., Combs, K.A., Kienzle, B., Ricci, B., Wager-Smith, K., Gil, C.M.,
1442 Turck, C.W., Bouma, M.E., Rader, D.J., et al. (1993). Cloning and gene defects in microsomal
1443 triglyceride transfer protein associated with abetalipoproteinaemia. Nature *365*, 65-69.

1444 Shoulders, C.C., Brett, D.J., Bayliss, J.D., Narcisi, T.M., Jarmuz, A., Grantham, T.T., Leoni,
1445 P.R., Bhattacharya, S., Pease, R.J., Cullen, P.M., et al. (1993). Abetalipoproteinemia is caused
1446 by defects of the gene encoding the 97 kDa subunit of a microsomal triglyceride transfer protein.
1447 Hum Mol Genet *2*, 2109-2116.

1448 Sim, N.L., Kumar, P., Hu, J., Henikoff, S., Schneider, G., and Ng, P.C. (2012). SIFT web server:
1449 predicting effects of amino acid substitutions on proteins. Nucleic Acids Res *40*, W452-457.

1450 Thierer, J.H., Ekker, S.C., and Farber, S.A. (In Press). LipoGlo: A sensitive and specific reporter
1451 of atherogenic lipoproteins. Nature Communications.

1452 Thompson, J.R., and Banaszak, L.J. (2002). Lipid-protein interactions in lipovitellin.
1453 Biochemistry *41*, 9398-9409.

1454 Van der Auwera, G.A., Carneiro, M.O., Hartl, C., Poplin, R., Del Angel, G., Levy-Moonshine, A.,
1455 Jordan, T., Shakir, K., Roazen, D., Thibault, J., et al. (2013). From FastQ data to high

1456 confidence variant calls: the Genome Analysis Toolkit best practices pipeline. Curr Protoc
1457 Bioinformatics *43*, 11 10 11-33.

1458 Vernier, J., and Sire, M. (1977). Lipoprotéines de très basse densité et glycogène dans le
1459 syncytium vitellin, l'épithélium intestinal et le foie, aux stades précoces du développement
1460 embryonnaire chez la truite arc-en-ciel. Biol. cell *29*, 45-54.

1461 Walsh, M.T., Di Leo, E., Okur, I., Tarugi, P., and Hussain, M.M. (2016). Structure-function
1462 analyses of microsomal triglyceride transfer protein missense mutations in abetalipoproteinemia
1463 and hypobetalipoproteinemia subjects. Biochim Biophys Acta *1861*, 1623-1633.

1464 Walsh, M.T., and Hussain, M.M. (2016). Targeting Microsomal Triglyceride Transfer Protein and
1465 Lipoprotein Assembly to Treat Homozygous Familial Hypercholesterolemia. Crit Rev. Clin. Lab
1466 Sci *54*, 26-48.

1467 Walsh, M.T., and Hussain, M.M. (2017). Targeting microsomal triglyceride transfer protein and
1468 lipoprotein assembly to treat homozygous familial hypercholesterolemia. Crit Rev Clin Lab Sci
1469 *54*, 26-48.

1470 Walsh, M.T., Iqbal, J., Josekutty, J., Soh, J., Di Leo, E., Ozaydin, E., Gunduz, M., Tarugi, P.,
1471 and Hussain, M.M. (2015). Novel Abetalipoproteinemia Missense Mutation Highlights the
1472 Importance of the N-Terminal beta-Barrel in Microsomal Triglyceride Transfer Protein Function.
1473 Circ Cardiovasc Genet *8*, 677-687.

1474 Walther, T.C., Chung, J., and Farese, R.V., Jr. (2017). Lipid Droplet Biogenesis. Annu Rev Cell
1475 Dev Biol *33*, 491-510.

1476 Walzer, C., and Schonenberger, N. (1979a). Ultrastructure and cytochemistry of the yolk
1477 syncytial layer in the alevin of trout (Salmo fario trutta L. and Salmo gairdneri R.) after hatching.
1478 II. The cytoplasmic zone. Cell Tissue Res *196*, 75-93.

1479 Walzer, C., and Schonenberger, N. (1979b). Ultrastructure and cytochemistry study of the yolk
1480 syncytial layer in the alevin of trout (Salmo fario trutta L.) after hatching. I. The vitellolysis zone.
1481 Cell Tissue Res *196*, 59-73.

1482 Wang, J., and Hegele, R.A. (2000). Microsomal triglyceride transfer protein (MTP) gene
1483 mutations in Canadian subjects with abetalipoproteinemia. Hum Mutat *15*, 294-295.

1484 Wang, Y., McLeod, R.S., and Yao, Z. (1997). Normal activity of microsomal triglyceride transfer
1485 protein is required for the oleate-induced secretion of very low density lipoproteins containing
1486 apolipoprotein B from McA-RH7777 cells. J Biol Chem *272*, 12272-12278.

1487 Wetterau, J.R., Aggerbeck, L.P., Bouma, M.E., Eisenberg, C., Munck, A., Hermier, M., Schmitz,
1488 J., Gay, G., Rader, D.J., and Gregg, R.E. (1992). Absence of microsomal triglyceride transfer
1489 protein in individuals with abetalipoproteinemia. Science *258*, 999-1001.

1490 Wetterau, J.R., Combs, K.A., Spinner, S.N., and Joiner, B.J. (1990). Protein disulfide isomerase
1491 is a component of the microsomal triglyceride transfer protein complex. J Biol Chem *265*, 9800-
1492 9807.

1493 Wetterau, J.R., Gregg, R.E., Harrity, T.W., Arbeeny, C., Cap, M., Connolly, F., Chu, C.H.,
1494 George, R.J., Gordon, D.A., Jamil, H., et al. (1998). An MTP inhibitor that normalizes
1495 atherogenic lipoprotein levels in WHHL rabbits. Science *282*, 751-754.

1496 Wetterau, J.R., and Zilversmit, D.B. (1984). A triglyceride and cholesteryl ester transfer protein
1497 associated with liver microsomes. J Biol Chem *259*, 10863-10866.

1498 Wetterau, J.R., and Zilversmit, D.B. (1985). Purification and characterization of microsomal
1499 triglyceride and cholesteryl ester transfer protein from bovine liver microsomes. Chem Phys
1500 Lipids *38*, 205-222.

1501 Wetterau, J.R., and Zilversmit, D.B. (1986). Localization of intracellular triacylglycerol and
1502 cholesteryl ester transfer activity in rat tissues. Biochim Biophys Acta *875*, 610-617.

1503 White, R.J., Collins, J.E., Sealy, I.M., Wali, N., Dooley, C.M., Digby, Z., Stemple, D.L., Murphy,
1504 D.N., Billis, K., Hourlier, T., et al. (2017). A high-resolution mRNA expression time course of
1505 embryonic development in zebrafish. Elife *6*.

1506 Wiegand, M.D. (1996). Composition, accumulation and utilization of yolk lipids in teleost fish.
1507 Reviews in fish biology and fisheries *6*, 259-286.

1508 Wu, X., Zhou, M., Huang, L.S., Wetterau, J., and Ginsberg, H.N. (1996). Demonstration of a
1509 physical interaction between microsomal triglyceride transfer protein and apolipoprotein B
1510 during the assembly of ApoB-containing lipoproteins. J Biol Chem *271*, 10277-10281.

1511 Yaniv, K., Isogai, S., Castranova, D., Dye, L., Hitomi, J., and Weinstein, B.M. (2006). Live
1512 imaging of lymphatic development in the zebrafish. Nat Med *12*, 711-716.

1513 Zeituni, E.M., Wilson, M.H., Zheng, X., Iglesias, P.A., Sepanski, M.A., Siddiqi, M.A., Anderson,
1514 J.L., Zheng, Y., and Farber, S.A. (2016). Endoplasmic Reticulum Lipid Flux Influences
1515 Enterocyte Nuclear Morphology and Lipid-dependent Transcriptional Responses. J Biol Chem
1516 *291*, 23804-23816.
1517